

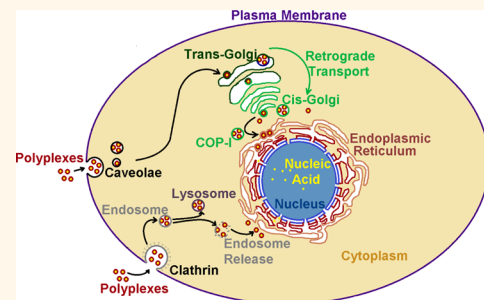


# Polymeric Nucleic Acid Vehicles Exploit Active Interorganelle Trafficking Mechanisms

Katy M. Fichter,<sup>†</sup> Nilesh P. Ingle,<sup>‡</sup> Patrick M. McLendon,<sup>§</sup> and Theresa M. Reineke<sup>‡,\*</sup>

<sup>†</sup>Department of Chemistry, Missouri State University, Springfield, Missouri, United States, <sup>‡</sup>Department of Chemistry, University of Minnesota—Twin Cities, Minneapolis, Minnesota, United States, and <sup>§</sup>Division of Molecular Cardiovascular Biology, Cincinnati Children's Hospital Medical Center, Cincinnati, Ohio, United States

**ABSTRACT** Materials that self-assemble with nucleic acids into nanocomplexes (e.g. polyplexes) are widely used in many fundamental biological and biomedical experiments. However, understanding the intracellular transport mechanisms of these vehicles remains a major hurdle in their effective usage. Here, we investigate two polycation models, Glycofect (which slowly degrades *via* hydrolysis) and linear polyethylenimine (PEI) (which does not rapidly hydrolyze), to determine the impact of polymeric structure on intracellular trafficking. Cells transfected using Glycofect underwent increasing transgene expression over the course of 40 h and remained benign over the course of 7 days. Transgene expression in cells transfected with PEI peaked at 16 h post-transfection and resulted in less than 10% survival after 7 days. While saccharide-containing Glycofect has a higher buffering capacity than PEI, polyplexes created with Glycofect demonstrate more sustained endosomal release, possibly suggesting an additional or alternative delivery mechanism to the classical “proton sponge mechanism”. PEI appeared to promote release of DNA from acidic organelles more than Glycofect. Immunofluorescence images indicate that both Glycofect and linear PEI traffic oligodeoxynucleotides to the Golgi and endoplasmic reticulum, which may be a route towards nuclear delivery. However, Glycofect polyplexes demonstrated higher co-localization with the ER than PEI polyplexes, and co-localization experiments indicate the retrograde transport of polyplexes *via* COP I vesicles from the Golgi to the ER. We conclude that slow release and unique trafficking behaviors of Glycofect polyplexes may be due to the presence of saccharide units and the degradable nature of the polymer, allowing more efficacious and benign delivery.



**KEYWORDS:** polyplex · intracellular trafficking · interorganelle · cationic polymer · gene therapy

The use of nucleic acids (NAs) to examine biological processes offers unprecedented possibilities for revolutionizing biological and medical research. Tools such as small interfering RNA (siRNA), oligodeoxynucleotides (ODNs), and plasmid DNA (pDNA) represent an effective means of modifying gene expression.<sup>1,2</sup> To exploit these tools, drug discovery now includes novel nanomedicine programs based on NA therapeutics that hold great promise for a variety of pathologies.<sup>3,4</sup> However, efficient cellular delivery and intracellular trafficking of NAs are a critical rate-limited step to their efficacy. While viral-mediated NA transfer is highly efficient, they are potentially more difficult to modify for various applications; thus, versatile methods to deliver a variety of nucleic acids would greatly benefit the field of nanomedicine.<sup>5</sup>

In response, creative design and development of synthetic, nonviral vehicles has been the subject of extremely vigorous research. Nonviral vehicles<sup>6</sup> are easier to synthesize and can accommodate a variety of nucleic acids,<sup>7</sup> and recent clinical work has shown they are well tolerated.<sup>4,8,9</sup> A wide variety of nonviral NA delivery vehicles with different chemical structures have been developed and extensively studied.<sup>10–16</sup> Many studies have demonstrated that the chemical structure of the vehicle plays a crucial role in their biological interactions.<sup>16–23</sup> In structure-based development, the ideal nonviral NA vehicle should target both a specific tissue type and a specific intracellular region or organelle while minimizing interference with native cellular processes. Therefore, understanding the influence of the chemical structure of NA vehicles on the intracellular delivery mechanisms is crucial to all

\* Address correspondence to treineke@umn.edu.

Received for review September 12, 2012 and accepted December 12, 2012.

Published online December 12, 2012  
10.1021/nn304218q

© 2012 American Chemical Society

researchers utilizing these materials and refining their structure toward clinical advancement.

Previous work has shown that cells internalize polyplexes (polymer–NA nanocomplexes) through many active cellular uptake mechanisms (*e.g.*, clathrin- and/or caveolae-mediated endocytosis and/or macropinocytosis).<sup>24–28</sup> While a multitude of endosomal trafficking pathways exist, the cell often routes exogenous materials toward the lysosomes, where enzymes degrade the therapeutic complexes, rendering them useless. Therefore, it has been proposed that escape from endocytic vesicles may be the largest barrier to intracellular efficacy.<sup>29–31</sup> To hypothesize upon the escape of polyplexes from lysosomes, the “proton sponge mechanism”<sup>10</sup> has been developed.<sup>29,32–34</sup> In brief, polymers with high H<sup>+</sup> buffering capacity (such as polyamines) are able to adsorb, or “sponge”, protons during acidification of the vesicle in which they are located. This theoretically results in vesicular accumulation of excess counterions, which subsequently cause osmotic swelling, leading to leaking or lysis of the endocytic vesicles.

However, vehicles employing the proton sponge mechanism have some notable drawbacks. Most notable is the high cellular toxicity associated with these vehicles, as they are typically membrane-lytic.<sup>35</sup> Additionally, NAs are released into the cytoplasm early in the transfection process, where they face degradation by nucleases in the cytoplasm.<sup>36</sup> Furthermore, after leaving endocytic vesicles, the NAs have little or no active transport to the target organelle; studies have shown that DNA intracellularly microinjected into the cytoplasm undergoes little to no diffusion.<sup>37,38</sup> Structural variations in synthetic nonviral vehicles could exploit alternative intracellular routes involving active trafficking of the NA nanocomplexes directly to the targeted organelle, which would greatly enhance their efficacy.

Several intracellular trafficking studies of polyplexes have concentrated on two routes that typically involve trafficking along actin and/or microtubules: (i) clathrin-mediated endocytosis,<sup>25,29,39–43</sup> and more recently (ii) caveolae-mediated endocytosis, which may facilitate higher nuclear delivery efficiency.<sup>11,39,44–47</sup> These pathways, however, are known to commonly sort macromolecules to organelles such as the Golgi and the endoplasmic reticulum (ER). Carbohydrate and saccharide residues are information-dense biomolecules; therefore the galactose residues in Glycofект could play a role in mediating the active transport of these polyplexes. Furthermore, because other glycosylated macromolecules, such as hormone receptors, have been shown to be transported from the ER to the nucleus, glycosylated NA delivery vehicles, such as Glycofект, may also be able to exploit the native intracellular trafficking pathways in the cell. Also, a recent study suggested that grafting of a nuclear

localization signal, histone H3, on a polyethyleneimine (PEI)-based delivery vehicle showed a significant preferential shift toward caveolae-mediated endocytosis and potential routing through the ER.<sup>45</sup> These promising new developments in synthesis and delivery of NA via nonviral polymeric delivery vehicles ratify the need for advanced designs. From a therapeutic perspective, polymer scaffolds are needed that promote efficient intracellular trafficking and sustained release of NAs. Here, we explore the potential of information-rich saccharide moieties on directing polyplex the caveolin-1 (CAV-1), Golgi, ER, and COPI vesicles (vesicles that traffic between the Golgi and ER); these pathways have potential to pave the way for efficient endocytosis, safe intracellular trafficking, and sustained NA delivery.

In the present study, we examine intracellular trafficking of polyplexes through sorting organelles such as the Golgi and ER in H9c2(2-1) (rat cardiomyoblast) cells; this work complements our previous work to understand intracellular trafficking pathways of polyplexes.<sup>50</sup> It should be noted that these routes are often exploited as infection pathways by viruses; it has been observed that cholera toxin and some viruses enter cells through caveolae-mediated endocytosis,<sup>48,49</sup> which often target the Golgi.<sup>50</sup> Current research also shows that polyplex trafficking through caveolae leads to high NA efficacy.<sup>47,51</sup> Once reaching the Golgi, COP I- and COP II-positive vesicles shuttle cargo between the ER and Golgi,<sup>52–55</sup> which is particularly interesting because the lumen of the ER is contiguous with the space between the inner and outer nuclear membranes.<sup>56</sup> While still incompletely understood, studies have uncovered active trafficking pathways of native glycosylated proteins between the ER and nucleus.<sup>57,58</sup> Because some delivery vehicles, such as Glycofект, contain saccharide moieties, similar intracellular pathways could also play a large role in delivery. Understanding how the vehicle structure mediates intracellular trafficking mechanisms could facilitate the *de novo* design of NA vehicles to exploit these native pathways, which could greatly increase delivery efficiency.

Herein, we use two model polycation delivery systems to investigate the active transport mechanisms described above. The first is a glycopolymer, (poly(galactaramidopentaethylenetetramine), Figure 1A). This polymer, previously published as G4 and structurally identical to the commercial reagent “Glycofект”, was characterized to contain nine repeat units and will hereafter be referred to as its commercial name, Glycofект, for simplicity. The other polycation used in this study is linear polyethyleneimine (commercial name: JetPEI, Figure 1B), which is structurally similar to Glycofект, minus the saccharide subunits. PEI is a charge-dense polycation that does not undergo hydrolysis and is widely used because of its high transfection efficiency, but often exhibits high cytotoxicity.<sup>59–61</sup>

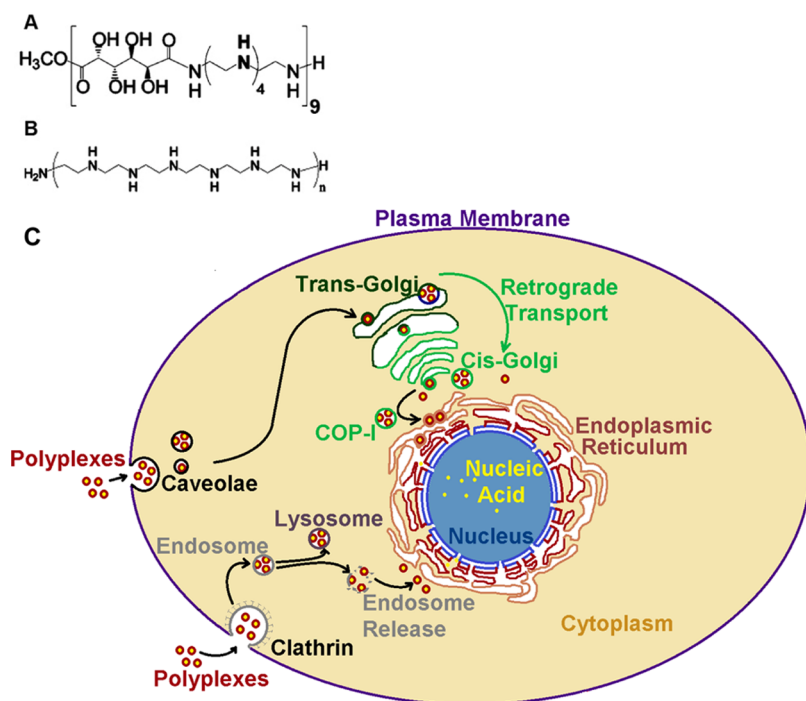


**Figure 1.** Structures of the two nonviral NA delivery vehicles examined herein and proposed intracellular pathways of study. (A) Poly(galactaramidopentaethylenetetramine), previously published as “G4” and commercially sold as “Glycofect”, is a degradable polymer ( $M_w = 4.6$  kDa; degree of polymerization,  $n = 11$ ).<sup>11</sup> (B) Linear PEI (commercially sold as “JetPEI”) is a nondegradable polymer  $M_w \approx 22$  kDa. (C) Proposed intracellular trafficking pathways of polyplexes.

Glycofect has demonstrated low toxicity, rapid degradation at neutral pH, and high NA transfer efficiency.<sup>11,20,62–67</sup> We demonstrate that polyplexes formed with Glycofect exploit an active transport pathway involving interorganelle transport *via* the Golgi and ER (Figure 1C) and that polymer structure mediates the kinetics and intracellular pathways of ODN delivery. Our results suggest that researchers can exploit efficient native interorganelle trafficking pathways by optimizing the chemical structure of polymer-based vehicles to target specific organelles. The analysis of these studies is crucial in tailoring future generations of nonviral NA vehicles.

## RESULTS

To investigate temporal changes in cellular delivery, H9c2(2-1) (rat cardiomyoblast) cells were transfected with (i) naked plasmid DNA (pDNA) (“no vehicle”), (ii) polyplexes formulated with linear PEI and pDNA, or (iii) polyplexes formulated with Glycofect and pDNA. In each case pDNA encoded the gene for luciferase, and the expression of this reporter gene was measured over the course of 7 days. Data from luciferase reporter gene assays are often reported in units of relative light units (RLU)/mg protein; however, the use of this unit may result in data interpretation artifacts because vehicles with high toxicity decrease in the amount of protein in each sample, falsely reporting higher “transfection efficiency”.<sup>11,62,65,66</sup> Data reported in Figure 2A depict the activity of the luciferase enzyme

in more straightforward terms by normalizing raw RLU values to the negative control (untransfected cells). For comparison, data in units of RLU/mg are also reported in Figure S1.

Figure 2A shows the transfection efficiency of PEI increases at early time points in the transfection process, peaks at 16 h, then decreases. Cells transfected with Glycofect show lower expression at early time points, but peaks above PEI at 40 h after transfection. Glycofect demonstrates almost a 2-fold increase in gene expression when compared to PEI at longer time points (4 and 7 days, Figure 2A, inset). Toxicity data for cells transfected with these vectors are depicted in Figure 2B and demonstrate the benign nature of Glycofect over the course of 7 days. PEI demonstrates excessive cellular toxicity, dropping to about 40% survival after 16 h and less than 10% survival after 7 days. These results support our hypothesis that Glycofect promotes slower, more efficacious and benign delivery of pDNA than linear PEI.

The proton sponge hypothesis predicts that the buffering capacity of the polymer is essential for endosomal escape and therefore plays a direct role in the transfection efficiency.<sup>10,68</sup> The buffering capacities of Glycofect and linear PEI were directly compared in solution with an amine concentration of 0.7744 M. This concentration was selected to model polymer concentration in intracellular endosomes in accordance with previously published reasoning.<sup>20</sup> The polymer solutions were titrated with HCl (hydrochloric acid) from

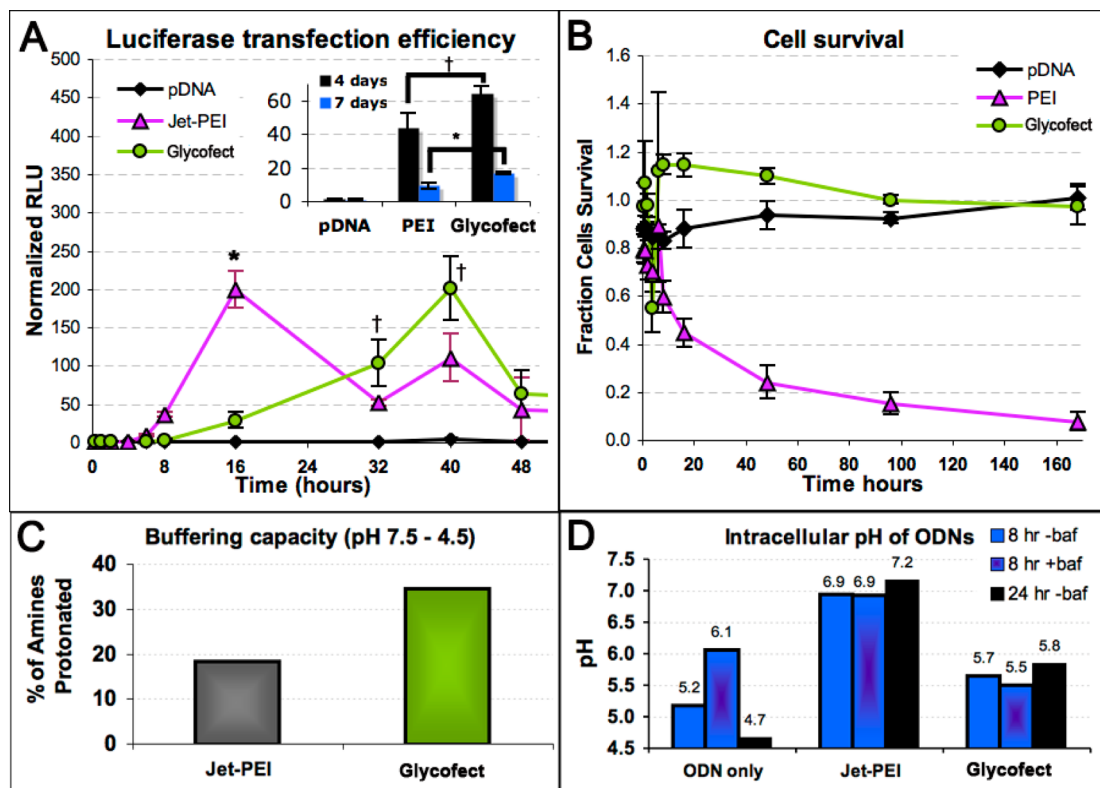


**Figure 2.** Biochemical characterization of PEI and Glycofект (A and B) H9c2(2-1) cells were transfected with luciferase pDNA and assayed for luciferase activity at the indicated time. Raw RLU values were normalized against untransfected cells; error is reported as SD of triplicate measurements. For comparison to units of RLU/mg, see Figure S1. \* $p < 0.01$  † $p < 0.05$ . (C) Buffering capacity of polyplexes reported as percent of amines protonated within the pH range 7.5–4.5. (D) Intracellular pH of ODNs at different time points and with or without (±) baflomycin during the transfection process. Intracellular pH calculations were derived using a standard curve (Figure S2). All transfections were performed with 5 N/P PEI and 20 N/P Glycofект.

pH 7.5 to 4.5, and the percent of amines protonated during the titration was calculated. These results demonstrate that the buffering capacity of Glycofект is much higher than that of linear PEI in this pH range (Figure 2C). The separation of the polyamine repeat units by saccharide residues, in the structure of Glycofект, may allow for an increased fraction of amine protonation (*i.e.*, the protonation of one amine electrostatically suppresses protonation of neighboring amines).<sup>20,64</sup>

To explore the role of buffering capacity on the ability of polyplexes to escape acidic vesicles, we measured the average pH environment of oligodeoxynucleotides within cultured cells *via* flow cytometry. H9c2(2-1) cells were transfected with dual-labeled ODNs, “FITC-ODN-Cy5” [*i.e.*, pH-sensitive FITC (fluorescein isothiocyanate) and pH-insensitive Cy5 (cyanine 5); see Materials and Methods]. Previous experiments have demonstrated that the fluorescence intensity ratio (FITC/Cy5) is linearly related to the pH environment of the ODN.<sup>29,69</sup> A linear calibration plot was created by measuring the FITC/Cy5 fluorescence intensity ratio of ODNs in transfected cells, suspended in intracellular clamping buffers (see Materials and Methods and Figure S2). Therefore, this calibration also accounts for any effect the complexed polymer may impart on fluorescence measurements.

We also investigated the effect of vesicular acidification on the intracellular pH of ODNs by treating cells with a vesicular proton pump inhibitor (baflomycin) and ion channel inhibitors (ionophores) 8 h after transfection. This experiment tested for evidence of a proton sponge mechanism in polymer–ODN delivery since the use of these drugs inhibits active vesicular acidification.<sup>70,71</sup> If the vehicle uses a proton sponge mechanism, the polymeric vehicles should be able to absorb excess protons in vesicles as allowed by their buffering capacity. Because we have measured the buffering capacity of Glycofект as higher than PEI, we would expect Glycofект to be able to absorb more protons than PEI, causing Glycofект–ODNs to be in a more pH-neutral environment.

Figure 2D depicts the intracellular pH environment of ODNs calculated from our flow cytometry measurements. It was observed that naked ODNs delivered without a vehicle (“ODN only”) were in acidic environments at both 8 and 24 h, presumably due to the inability to escape actively acidifying vesicles (and the lack of vehicle with buffering amines). However, the pH environment of the naked ODNs increases with the addition of baflomycin and ionophores, which was expected since most ODNs resided in acidic environments and the presence of these additives inhibits the

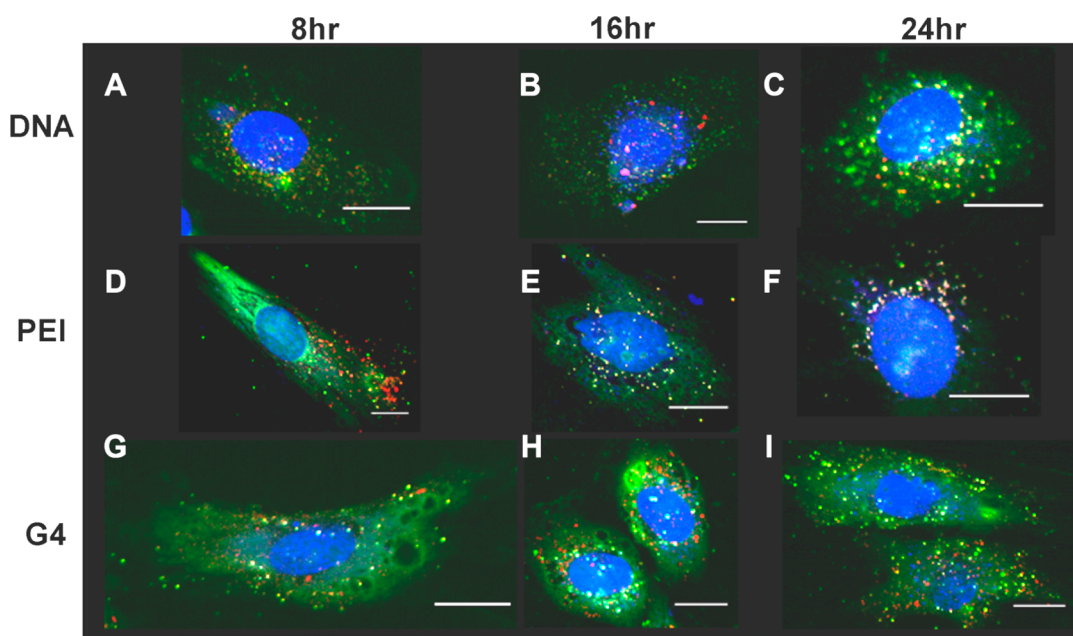


**Figure 3.** Micrographs of transfected H9c2(2-1) cells with time. Cells were transfected using naked ODN (A–C), PEI–ODN polyplexes at 5 N/P (D–F), or Glycofect (G4)–ODN polyplexes at 20 N/P (G–I) and fixed at the indicated time. FITC ODNs (green), LysoTracker (red), Draq5 (blue). The confocal pinhole was opened to capture a  $1.5\text{ }\mu\text{m}$  vertical slice in order to observe the diffuse cytoplasmic location of ODNs. Scale bar =  $20\text{ }\mu\text{m}$ .

proton pumps. The intracellular pH of ODNs delivered with PEI was neutral after both 8 and 24 h, suggesting that the majority of PEI–ODN polyplexes exist in pH-neutral subcellular environments (*e.g.*, the cytoplasm or neutral organelles). As expected, the pH environment of PEI–ODN complexes did not change upon baflomycin treatment because the pH environment of these PEI–ODNs was neutral without baflomycin treatment. The average intracellular pH of Glycofect–ODN complexes was 5.7 after 8 h and did not significantly change after 24 h (pH = 5.8). Surprisingly, the pH environment of Glycofect–ODN complexes did not significantly change with baflomycin treatment (from 5.7 to 5.5).

These measurements of ODN intracellular pH environments demonstrate that, while the buffering capacity of Glycofect is higher than that of linear PEI (Figure 2C), the average pH environment of Glycofect–ODNs is lower in all conditions tested, suggesting that Glycofect may not employ the proton sponge mechanism as a major mechanism of ODN delivery. At the same time it should be noted that slower kinetics of buffering behavior for Glycofect polyplexes and an effect of polymer hydrolysis (causing the liberation of galactartic acid and pentaethylenehexamine) could also be hypothesized to result in delayed  $\text{H}^+$  buffering of endosomes. Because the subcellular pH environment of Glycofect-delivered ODNs is unaffected by baflomycin treatment, we speculate that Glycofect polyplexes may dwell in a mixture of subcellular compartments, actively acidifying vesicles, slightly acidic organelles (*i.e.*, early endosomes, Golgi apparatus, endoplasmic

reticulum), and pH-neutral environments (*i.e.*, cytoplasm, nucleus), decreasing the effect of the baflomycin treatment on overall ODN pH. Conversely, pH measurements indicate that PEI delivers ODN to pH-neutral environments within 8 h. This may result *via* a combination of proton-sponge-mediated release of ODN to neutral compartments and disruption of membranes due to direct contact with PEI, causing the leaking of polyplexes out of vesicles. It has been previously demonstrated that charge-dense vehicles such as PEI are very damaging to biological membranes<sup>60,72,73</sup> and, therefore, may be exploited by this vector to facilitate rapid release of the ODNs into the cytoplasm, either directly from the plasma membrane or from intracellular vesicles. A large body of work by our lab and others supports these results, demonstrating that vehicle buffering capacity does not necessarily correlate to delivery or transfection efficiency.<sup>20,74,75</sup>

Because our intracellular pH data from flow cytometry is able to provide only an average pH of ODNs in a large population of cells, microscopy was used to observe different subcellular populations of ODNs colocalized with acidic vesicles. Micrographs in Figure 3 depict the typical staining pattern of FITC-labeled ODN in transfected H9c2(2-1) cells, using LysoTracker to visualize acidic vesicles. Cells were fixed and mounted in pH-neutral mountant prior to imaging to avoid quenching of FITC fluorescence in acidic compartments. Cells transfected without a transfection reagent (Figure 3A–C) generally exhibit punctate staining without a significant amount of cytoplasmic ODN staining, which correlates with our previous data

(Figure 2D) that show these ODNs remain in acidifying vesicles.

In cells transfected with PEI (Figure 3D–F) we observed that the cytoplasm was brightly and diffusely stained with ODN 8 h after transfection. This correlates with our previous data indicating that PEI delivers the majority of ODN to a neutral pH environment within 8 h (Figure 2D). Afterward, the cytoplasmic ODN distribution faded and a significant amount of ODN was observed in the nucleus after 24 h (Figure 3F and Figure S3). It should be noted that at both 16 and 24 h some perinuclear co-localization of FITC–ODN with Lysotracker is observed (Figure 3E, F); however, the average intracellular pH measurements indicate that the majority of ODNs reside in pH-neutral environments (Figure 2D). Additionally, it is not clear from these microscopy studies if the ODNs co-localized with Lysotracker in Figure 3E and F are still associated with PEI. Overall, these results support our observations that PEI encourages quick release of the majority of ODN into the cytoplasm of the cell within 8 h.

Cells were then transfected with Glycofect under identical conditions and imaged (Figure 3G–I). A mixed intracellular population of ODNs was found, which may explain our average intracellular pH measurements (Figure 2D). For example, one subset of ODNs appeared punctate (*e.g.*, in membrane-bound vesicles) and another subset appeared to be diffuse throughout the cell (*e.g.*, in the cytoplasm), which could result in a persistent slightly acidic (pH ~5.7) average measurement. Polyplexes formulated with Glycofect and ODNs appeared to accumulate in the nucleus of some cells by 16 and 24 h. Importantly, a diffuse, cytoplasmic fraction of ODNs delivered with Glycofect persists over the course of 24 h, suggesting the ability of Glycofect to mediate sustained cytoplasmic ODN delivery.

To corroborate these microscopy studies, a flow cytometry-based Acridine Orange (AO) assay<sup>76</sup> was performed to examine the ability of polymeric vehicles to initiate ODN escape from lysosomes. In this assay, AO partitions into intact acidic organelles and fluoresces brightly in these acidic environments. When the membrane integrity of an acidic organelle is compromised (*e.g.*, due to damage to or lysis of membranes by polymeric vehicles), vesicles can no longer maintain an internal acidic environment, and average AO fluorescence is quenched (diminished). Our results show that acidic vesicles remain intact in nontransfected cells and cells transfected with naked DNA over the course of 24 h, which is expected since no vehicle is present to induce membrane rupture (Figure S4). In contrast, cells transfected using PEI exhibit some lysis of acidic organelles, starting at 8 h post-transfection in up to 6% of the cells, indicating a small percentage of cells with significant vesicle lysis. This is consistent with microscopy data in Figure 3D–F, which show diffuse

cytoplasmic presence of ODNs along with some lysosomal co-localization. Cells transfected with Glycofect, however, do not exhibit significant lysosomal lysis over the course of 24 h and yield similar results to ODN only. While our microscopy data indicates that some Glycofect-delivered ODN is present in lysosomes, these data correlate with our previous experiments and suggest that Glycofect may not employ a “proton sponge” mechanism of endosomal/lysosomal escape and may use an alternate mechanism.

Actin is implicated in every known form of active endocytosis,<sup>77</sup> including clathrin- and caveolae-mediated endocytosis,<sup>78,79</sup> macropinocytosis,<sup>80</sup> and other, less characterized forms of endocytosis.<sup>81</sup> To investigate the role of actin on the cellular uptake of polyplexes, we disrupted actin polymerization with cytochalasin D (Figure S5A). In addition, we also inhibited uptake *via* caveolae (using Filipin III) and uptake *via* clathrin (using chlorpromazine), to delineate specific information about the primary pathways of polyplex uptake (Figure S5B, C) in this cell type.<sup>82</sup> Glycofect ODN uptake slightly decreased with actin depolymerization, and PEI–ODN uptake slightly increased with the same, although this difference was not significant (Figure S5A). Additionally, both clathrin and caveolae appeared to be major internalization routes for Glycofect and PEI, but the inhibition of clathrin- and caveolae-mediated endocytosis was more pronounced for Glycofect polyplexes, possibly suggesting the involvement of poorly characterized or nonendocytic import mechanisms for PEI. These data are in agreement with previous findings from our lab and work by other researchers in this field.<sup>47,51</sup> In a directly related previous study, we reported that the structure of the polymer (responsible for the chemical interactions with the cell surface and net charge on the surface of the polyplex) significantly influences interaction with a variety of cell surface glycosaminoglycans (GAGs) on HeLa cells and also appears to play a major role in the cellular uptake efficiency of both Glycofect (previously published as G4) and JetPEI.<sup>83</sup> In that study, it was found that sulfated GAGs are required for cellular internalization of Glycofect polyplexes but not for JetPEI and that hyaluronic acid and heparin sulfate were the primary GAGs that bound in the strongest manner to Glycofect polyplexes.

To investigate polyplex internalization at a subcellular level, we performed immunocytochemistry (ICC) experiments. In cells transfected with Glycofect–ODN complexes, minimal co-localization was observed between FITC–ODN and clathrin, indicating that ODNs delivered with Glycofect are not associated with clathrin-coated vesicles at this late (24 h) time point (Figure 4A, top). This was expected, since the clathrin coat is removed from internalized vesicles within minutes of internalization.<sup>84</sup> Despite previous data

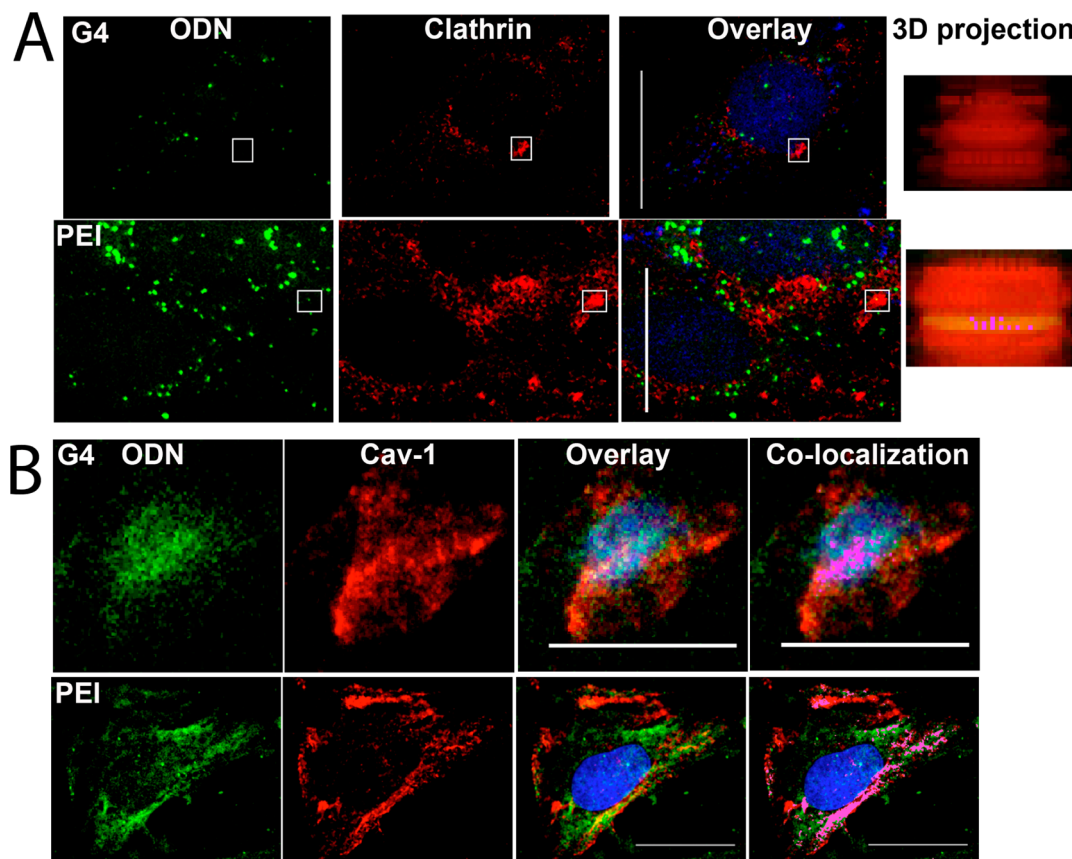


**Figure 4. Co-localization of ODNs delivered by PEI (5 N/P) or Glycofect (20 N/P) with clathrin or caveolin-1.** (A) H9c2(2-1) cells were transfected with FITC-ODN; 24 h later, cells were fixed and immunostained for clathrin. The 3D projection depicts a budding clathrin pit, located at the indicated boxed area in the maximum projection image. The top of the 3D projection image is near the plasma membrane, and the bottom of the image is the bottom of the coated pit. Magenta pixels indicate co-localization. (B) Cells were transfected as in A and stained for caveolin-1. Scale bars = 20  $\mu$ m.

suggesting that uptake of linear PEI (polymer only; no DNA) is independent of clathrin,<sup>85</sup> a small degree of co-localization was observed between PEI-delivered ODNs and clathrin-coated vesicles 24 h post-transfection (Figure 4A, bottom). Previous studies have demonstrated that DNA delivered with PEI can be exocytosed,<sup>28</sup> a process that can also involve clathrin; therefore this observation could also be due to the cellular export of exogenous DNA.

We also used ICC to investigate co-localization between caveolae and FITC-ODN in cells 24 h after transfection (Figure 4B). Significant co-localization was observed between caveolin-1 and ODN delivered with both polymers. These results agree with our caveolae inhibition studies and suggest a role for caveolae in polyplex uptake (Figure S5C). Caveolin-1 is found on the plasma membrane, Golgi complex, endoplasmic reticulum, and vesicles that bud from these organelles.<sup>79</sup> Therefore the co-localization of ODN and caveolin-1 suggests that both Glycofect and PEI polyplexes could engage in interorganelle trafficking between caveolin-associated organelles (e.g. Golgi, ER). While many studies have shown polyplexes are internalized by multiple avenues of endocytosis,<sup>39,47</sup> a caveolin-mediated endocytic gateway may guide a subset of polyplexes

to caveolin-associated organelles. This observation may represent a newly discovered active route of intracellular transport that could enhance transfection efficiency, due to the spatial proximity of these organelles with the nucleus and the known trafficking routes between these organelles.<sup>45</sup>

Cellular internalization of polyplexes by caveolae and clathrin-mediated uptake can lead to trafficking to many different organelles within the cell. One possible destination, particularly associated with caveolae-mediated trafficking, is the Golgi complex, the primary packaging and sorting apparatus in the cell for biomolecular cargo. The interior of the Golgi complex is maintained at a slightly acidic pH (~6.2–6.6);<sup>86,87</sup> therefore polyplex transport to this organelle could partially contribute to the slightly acidic average pH environment (~5.7) measured with Glycofect-delivered ODN (Figure 2D). Co-localization between FITC-ODN and the Golgi complex was examined in H9c2(2-1) cells 24 h post-transfection via ICC with giantin, a transmembrane protein of the Golgi complex (Figure 5A and B). A small amount of ODN delivered with PEI was observed as uniformly small puncta co-localized with the Golgi complex (Figure 5A and B, bottom row). ODN delivery with Glycofect (Figure 5A

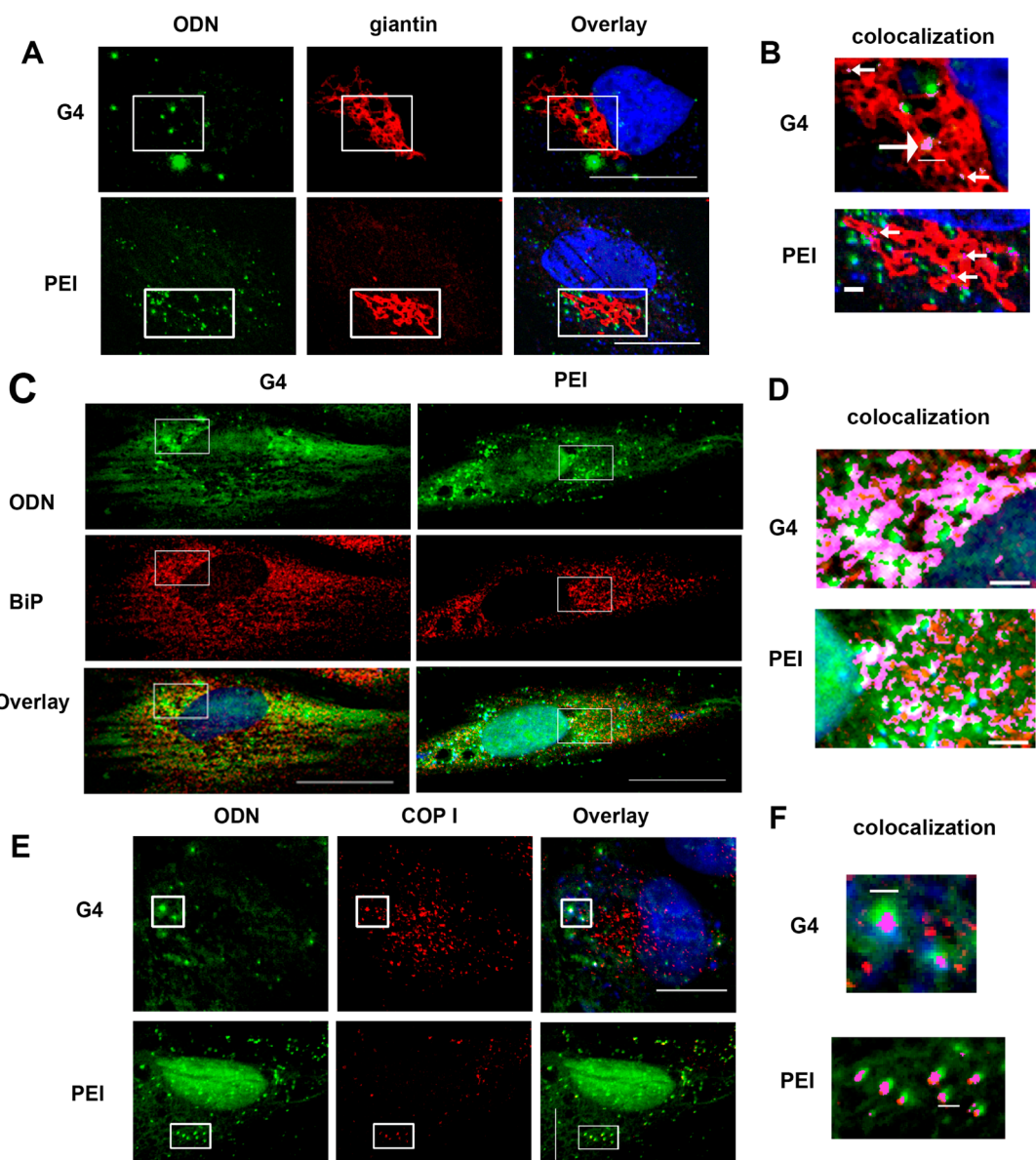


**Figure 5.** H9c2(2-1) cells were transfected with FITC–ODN using linear PEI (5 N/P) or Glycofect (G4, 20 N/P). Twenty-four hours after transfection, cells were fixed, permeabilized, and labeled for the indicated organelle marker using immunofluorescence. The boxes depicted in A, C, and E are shown in B, D, and F, respectively, with co-localized pixels indicated in magenta. (A and B) Co-localization between FITC–ODN and giantin (Golgi complex). (C and D) Co-localization between FITC–ODN and BiP (ER lumen). (E and F) Co-localization between FITC–ODN and  $\beta$ COP I (Golgi complex-derived vesicles). Scale bar in A, C, and E = 20  $\mu$ m. Scale bar in B, D, and F = 2  $\mu$ m.

and B, top row) also co-localized with the Golgi complex; however, puncta of ODN delivered with Glycofect were observed to have a more diverse size range than those of PEI-delivered ODN (Figure 5B, arrows). These data support the hypothesis that the Golgi complex may play a role in polyplex sorting and transport throughout the cell.

The endoplasmic reticulum is another known destination for caveolae-mediated trafficking. Because the lumen of the ER is contiguous with the space between the inner and outer nuclear envelope, trafficking of nucleic acids to the ER could be an intermediate in the mechanism of transport to the nucleus. Related work as indicated cellular trafficking of glycosylated

proteins from the ER to the nucleus,<sup>57,58</sup> and such a pathway could play a role in polyplex transport. To examine the involvement of the ER in nucleic acid trafficking, ICC was used to observe co-localization between FITC–ODN and BiP (a luminal ER protein), 24 h after transfection. Significant co-localization was observed between the ER and ODNs delivered with both PEI and Glycofect (Figure 5C and D). To quantitate the degree of co-localization between the ER and ODNs delivered with both polymers, the Manders coefficient<sup>88</sup> was calculated using the boxed area in Figure 5C (enlarged in Figure 5D). The Manders coefficient can be used to analyze the degree of overlap between pixels from two different channels and ranges

from 0 to 1, where 0 correlates to virtually no overlap and 1 correlates to virtually complete overlap. The M1 coefficient (green pixels overlapping red) was found to be 0.889 for Glycofect-transfected cells and 0.457 for PEI-transfected cells. These values suggest the degree of co-localization between Glycofect-delivered ODNs and the ER is twice as much as the degree of co-localization between PEI-delivered ODNs and the ER, which is additional evidence of an alternate delivery pathway for Glycofect, a polymeric vehicle containing saccharide moieties.

To investigate active interorganelle trafficking pathways of polymer-delivered ODNs, we used ICC to investigate ODN co-localization with COPI vesicles, which are responsible for retrograde cargo transport from the *cis* end of the Golgi to the rough ER. These experiments indicate that ODNs delivered with both polymers co-localize with COPI-coated vesicles 24 h after transfection (Figure 5E and F).

These data support our hypothesis that polyplexes undergo active interorganelle transport. Specifically, these studies suggest potential active interorganelle routes of transport to the ER: (i) *via* caveolin-associated vesicles<sup>89</sup> and/or (ii) *via* COPI vesicles from the Golgi complex.<sup>52</sup> While only a small degree of co-localization was observed between the Golgi and ODNs 24 h after transfection, it is possible that co-localization between ODNs and this organelle could be higher at earlier time points. It should also be noted that this organelle is used for sorting, and so localization at this organelle will be transient. Trafficking *via* the ER is particularly interesting because the spatial proximity of exogenous DNA to the nucleus is enhanced due to the congruency of the ER lumen with the space between the inner and outer nuclear membrane. This could potentially lead to a route of nuclear transport of nonviral vehicles, which is common for glycosylated proteins in the cell.<sup>57,58</sup> We have previously shown that multiple mechanisms of cellular uptake are implicated in polymer-mediated DNA delivery.<sup>47</sup> These results are corroborated here, especially with regard to caveolae-mediated trafficking pathways, which may provoke the involvement of the Golgi complex and ER. More broadly, our results suggest that polymer structure plays a critical role in the intracellular routes through which exogenous DNA is trafficked, with potentially profound effects on their efficacy and cytotoxicity.

Collectively, the average pH environment polymer-delivered ODNs (Figure 2D) and identification of organelles implicated in ODN trafficking (Figures 3–5) suggest alternative trafficking pathways to the classical “proton sponge mechanism”. We built on these data by investigating the subcellular pH environments of ODNs delivered with Glycofect and linear PEI, *via* live-cell time-lapse microscopy to visualize spatial and temporal changes in subcellular pH environments of ODNs. Similar to the average intracellular pH data presented in Figure 2D, the pH environment of ODNs

can be assessed at a subcellular level *via* fluorescence microscopy. Figure 6 summarizes these experiments in which H9c2(2-1) cells were transfected with double-labeled (FITC-Cy5) ODNs. Because FITC (pseudocolored in green) quenches in low pH environments, pixels representing ODNs in acidic environments ( $\text{pH} < \sim 5.0$ )<sup>90</sup> have lower, or absent, green intensity. Conversely, in neutral pH environments, FITC fluoresces brightly and pixels in the green channel have high pixel intensity. Because Cy5 fluorescence (pseudocolored in blue) is not affected by pH, the ratio (FITC/Cy5) of pixel intensity in the images can be used to infer the relative pH environment of the ODNs.

Figure 6A depicts a live H9c2(2-1) cell 4 h after transfection with FITC-ODN-Cy5 using Glycofect (see also Figure S6A). In the left-most image of Figure 6A, the boxed area is shown at different time points in smaller insets to the right. Consistent with the pH assays (Figure 2D), most FITC-ODN-Cy5 appears blue, indicating most ODNs are in a subcellular environment with a pH around 5. However, the time-lapse movie of this cell (Movie S1) reveals that there are dynamic populations of FITC-ODN-Cy5 in a range of pH environments. Sporadic motion of the puncta is consistent with trafficking along actin or microtubules. The boxed images on the right of Figure 6A show large clumps of ODN, which may be polyplexes in the process of being endocytosed. Thirty hours after transfection with Glycofect (Figure 6B), a subpopulation of slightly acidic (blue-green) ODNs emerges, indicating that they have been trafficked to more neutral pH environments (see also Movie S2). A striking feature of this image is the large green regions of FITC-ODN-Cy5 (*i.e.*, in pH-neutral environments), one of which appears to possibly leak small amounts of fluorescent DNA out of a compartment with time (Movie S2).

Figure 6C shows an H9c2(2-1) cell transfected using PEI–ODN polyplexes 4 h post-transfection. In general, when compared to Glycofect-delivered ODNs at 4 h (Figure 6A), a greater fraction of PEI-delivered ODNs appear to be in pH-neutral environments. However, similar to Figure 6A, ODNs in neutral pH environments are located near the plasma membrane. These pH-neutral ODNs may represent polyplexes on the cell surface, actively undergoing uptake, or in early stages of endocytosis. The time-course movies of PEI-delivered ODN trafficking after 4 h (Movie S3) corroborate this hypothesis: vesicles containing this ODN appear to traffic toward the center of the cell and decrease in green intensity (undergo acidification).

After 30 h of transfection, PEI-delivered ODNs can be classified into three subpopulations: (1) in pH-neutral environments within the nucleus, (2) in mildly acidic environments, accumulated in the perinuclear region, and (3) in pH-neutral environments near the cell periphery (Figure 6D). This third subpopulation of ODNs does not appear to be moving into the cell and may

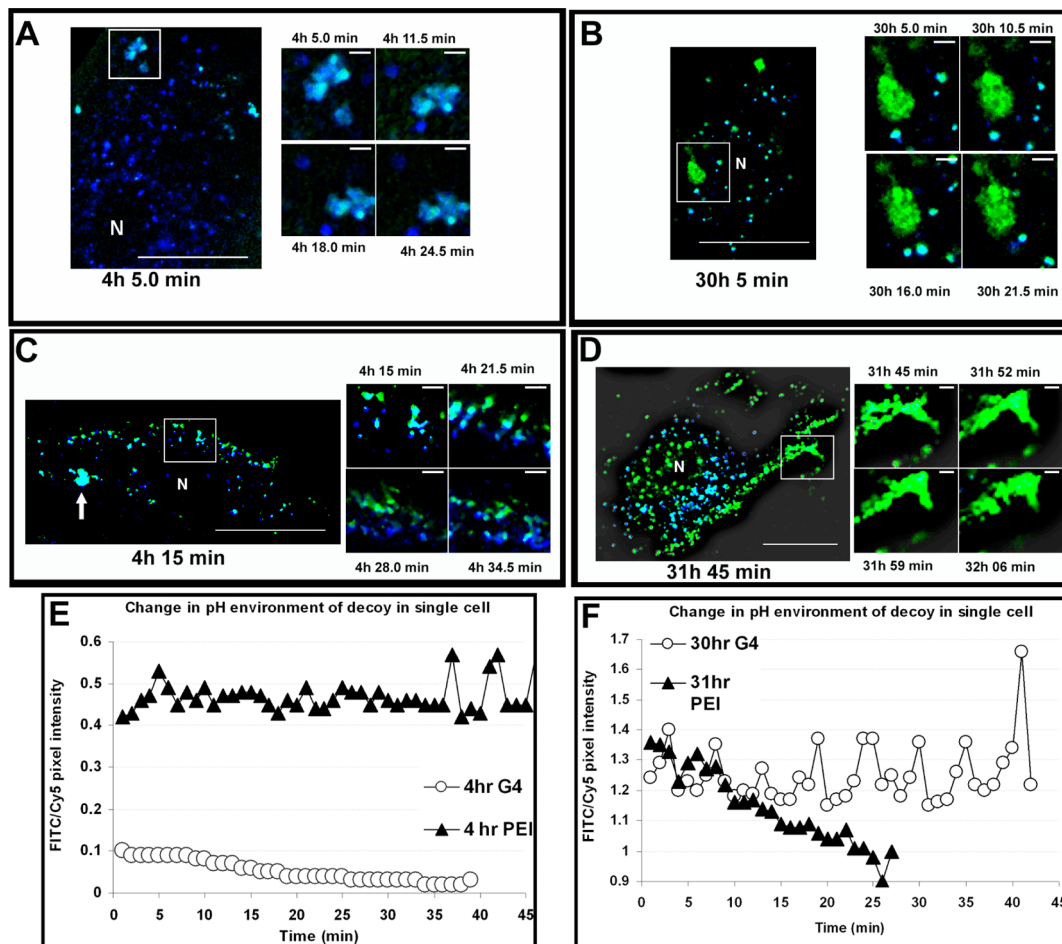


**Figure 6.** Confocal images of live H9c2(2-1) cells transfected with double-labeled FITC (green)-Cy5 (blue) ODNs and polyplexes formulated with either the Glycofect (20 N/P) or PEI (5 N/P). (A) FITC/Cy5-ODNs delivered with Glycofect after approximately 4 h. (B) FITC/Cy5-ODNs delivered with Glycofect after approximately 30 h. (C) FITC/Cy5-ODNs delivered with PEI after approximately 4 h. (D) FITC/Cy5-ODNs delivered with PEI after approximately 30 h. Insets are time-lapse micrographs of the indicated boxed area. Scale bar = 20  $\mu$ m in large images and 2  $\mu$ m in inset images. The letter "N" denotes the nucleus. (E and F) Changes in mean pH environment of ODNs in a single cell with time. The average pixel intensity of FITC and Cy5 was measured at each time point, and the ratio was plotted against time. (E) 4 h post-transfection. (F) 30 h post-transfection.

represent ODN leaking out of the cell (Movie S4, arrow). Many studies have demonstrated that PEI induces plasma membrane damage *via* charge interactions<sup>73,91</sup> and that PEI is capable of damaging intracellular membranes from the cytosolic face.<sup>92</sup> In light of this evidence, PEI may also cause endosomal release *via* membrane damage (in addition to the proton sponge mechanism). This potential for membrane damage could result in damage to the inner face of the PM causing DNA to leak from the cell (see DIC overlay image Figure S6D). We speculate that this may be observed in Movie S4 (and Figure 6D, right) where the arrowhead depicts the location of what could be leaking of ODN from the cell.

To analyze temporal changes in the pH environments of ODNs from our ratiometric fluorescence microscopy experiments, the FITC/Cy5 pixel intensity ratio was plotted with time. As previously mentioned, this ratio can be inferred as the relative subcellular pH environment of ODNs. Figure 6E shows these plots

over the course of about 45 min, starting 4 h after transfection. As observed, the pH environment of Glycofect-delivered ODNs was lower than that of PEI-delivered ODNs, which is consistent with average intercellular pH measurements in Figure 2D. After about 4.5 h post-transfection (35 mins after data collection started), ODNs delivered with PEI exhibit a spiking pattern (Figure 6E), which may be indicative of short bursts of ODNs rapidly encountering a neutral pH environment at this early point in the transfection process, which is consistent with the diffuse cytoplasmic distribution observed of PEI-delivered ODNs at 8 h post-transfection in Figure 3D. As the FITC-ODN-Cy5 diffuses into the cytosol and out of the focal plane depicted in the images, the plot returns to baseline.

Figure 6F shows plots of the ODN pH environment over the course of 45 min, starting at approximately 30 h post transfection. PEI-delivered ODN demonstrates a sharp decline in average relative pH.

This evidence agrees with our hypothesis that the peripheral population of neutral ODN may be leaving the cell (potentially through damage to the plasma membrane or exocytosis) and/or being further acidified en route elsewhere in the cell, decreasing the overall ODN pH environment. In contrast, after 30 h of Glycofect-mediated delivery, ratiometric measurements demonstrated a relatively stable, higher pH environment. However, the average pH environment of Glycofect-delivered ODNs fluctuated, exhibiting a similar spiking pattern seen in the plot of PEI-delivered ODNs after 4.5 h of transfection (Figure 6F, open circles). These results also may be interpreted as sustained release of ODN from acidic compartments at later time points, which corroborates our hypothesis of prolonged and sustained cytosolic delivery of ODN. The temporal ratiometric fluorescence movies of Glycofect-delivered ODN (Movies S1 and S2) further support our suggestion that Glycofect-mediated ODN trafficking appears to follow an active vesicular transport mechanism within the cell at later time points. Together, these time-lapse ratiometric fluorescence measurements support our previous data demonstrating slower, prolonged, and sustained active intracellular trafficking of ODNs delivered with Glycofect *versus* PEI.

## DISCUSSION

Nucleic acid delivery has exhibited tremendous potential both for therapeutic use, as well as a tool to understand fundamentals of normal biological processes and disease. While it is well known that the vehicle structure plays a large role in the delivery mechanisms, kinetics, efficacy, and toxicity, relatively little is known about how this impacts the intracellular pathways employed by polymer-based vehicles to carry nucleic acids to their desired intracellular location. Knowledge of these pathways will help researchers to develop vehicles that can efficiently carry their nucleic acid cargo through specific intracellular routes while remaining benign to the cell. To this end, we have examined the intracellular routes taken by two model polymeric vehicle types, linear PEI and Glycofect.

In cells transfected with PEI, we have shown that transgene expression occurs quickly, yet decreases as cellular survival drops drastically, starting at 16 h after transfection. In contrast, while Glycofect mediates slower transfection efficiency, it exhibits sustained cytoplasmic release and extended delivery to intracellular organelles and remains benign to cells in culture over the course of at least 7 days. Additionally, we have shown that PEI-delivered ODN is more quickly transported to pH-neutral intracellular environments, despite the lower buffering capacity of this vehicle as compared to Glycofect (Figure 2C). Furthermore, our subcellular fluorescence microscopy studies demonstrate delayed, but more sustained release of Glycofect-delivered ODN

to the cytosol, both with pH-based measurements (Figures 2D and 6) and subcellular co-localization with acidic organelles (Figure 3). These results contribute to and correlate with a body of previously published work that scrutinize the traditionally held “proton sponge mechanism” of endosomal release.<sup>10</sup> In addition, at 4, 8, and 24 h post-transfection, average intracellular ODN pH is more acidic with Glycofect (Figures 2D and 6A, E), when compared to data at the same time points with linear PEI (Figures 2D and 6C, E). This acidic environment would normally suggest that the polyplexes may be located inside either late endosomes or lysosomes; however, upon further exploration, we found this was not the case. Further studies (Figure S4, Supporting Information) indicate that PEI has a slightly higher ( $p < 0.05$ ) tendency to rupture acidic vesicles as compared to Glycofect as measured by an AO assay in whole cells. These data suggest that PEI polyplexes may be sequestered in and rupture these acidic vesicles,<sup>10,68,69</sup> more so than Glycofect. Additionally, other studies by our group and others have shown that the tendency of PEI-based polyplexes to cause membrane rupture also causes significant cellular toxicity.<sup>35,60,93</sup> Together these results suggest that vesicle release of polyplexes into the cytoplasm occurs by different mechanisms depending on vehicle structure. We demonstrate evidence that a subset of the Glycofect polyplex population that may be shuttled to other slightly acidic regions within the cell (Figure 5). Glycofect polyplexes also appeared to remain in vesicles over longer time periods (Figures 3 and 6), potentially due to the structural design of this polymer, which could possibly be responsible for two primary functions: (1) protect the complexed ODN from acidic milieu (*via* both NA encapsulation and the higher buffering capacity than PEI, Figure 2C) and (2) promote regulated sustained release of ODN in the perinuclear region of a cell due to degradation of the vehicle.<sup>67</sup> Figure 2D and Figure 3G–I corroborate this possible sustained release in the perinuclear region of a cell. Thus, Glycofect polyplexes may have a higher portion of intact nucleic acid in the active transport pathway in the cell; our experiments demonstrate that between 40 h up to 4 d Glycofect-mediated ODN delivery also leads to more sustained gene expression (Figure 2A).

Despite the fact that Glycofect has a higher buffering capacity than PEI, the overall subcellular pH environment of Glycofect-delivered ODN is more acidic than PEI. These results, as well as results obtained by our lab and others, have shown that higher buffering capacity does not necessarily directly correlate to higher gene expression.<sup>94–96</sup> This observation lead us to hypothesize that PEI polyplexes may be trafficked through acidic organelles,<sup>29,43,45</sup> while cells may favor trafficking Glycofect polyplexes through an alternative pathway(s) distinct from the “proton sponge” mechanism.

In recent studies by our group, we have demonstrated that PEI induces plasma membrane permeabilization within the first 30 min of transfection and nuclear membrane permeabilization by 4 h post-transfection, which results in higher cellular toxicity. Many other groups have also shown evidence that PEI can cause damage to cellular membranes.<sup>60,97</sup> After 4 h, PEI present in the cell could also permeabilize other intracellular organelles, such as mitochondria, causing further toxicity.<sup>35,98</sup> Thus, we hypothesize that the higher gene expression of PEI vehicles at earlier time points may be partly attributed to physical membrane disruption.<sup>98</sup> Multiple membrane damage events, both at the plasma membrane and inside the cell, have been shown to trigger apoptosis and could be a primary means of material toxicity and cell death.<sup>35,46,98,99</sup> In contrast, Glycofект polyplexes are relatively nontoxic and show sustained gene expression levels up to 48 h (Figure 2A). This observation strongly corroborates the hypothesis of this study: that Glycofект begins to moderate the critical balance between toxicity and gene expression by routing cellular trafficking of polyplexes through native active intracellular routes (e.g. via Golgi and ER).

The slower kinetics of delivery promoted by Glycofект and the generally acidic pH environment experienced by Glycofект polyplexes inspired us to investigate the alternative active transport pathways in the cell. Inhibiting clathrin and caveolae-mediated endocytosis strongly decreased cellular uptake of both PEI–ODN and Glycofект–ODN, indicating these pathways are major routes of transit in H9c2(2-1) cells, which supports previous work completed by our group and others.<sup>45,47,51,83</sup> An important finding of this study obtained with the positive co-localization data of ODN with the Golgi, ER, and COPI vesicles (Figures 4 and 5) supports our hypothesis that the innate sorting routes in cells are used to transport exogenous nucleic acids delivered with nonviral vehicles. In particular, the strong co-localization of Glycofект–ODNs with the ER along with the slower delivery kinetics is intriguing and could indicate that a higher portion of Glycofект-delivered ODNs are transported *via* interorganelle transit. While the co-localization/trafficking results are similar for linear PEI and Glycofект, the difference in kinetics and stronger ER localization with Glycofект suggest that that Glycofект could rely more heavily on this mechanism.<sup>47</sup>

Live cell confocal microscopy (Figure 6) provides evidence, albeit indirect, to support the hypothesis that PEI can induce intracellular membrane damage as a possible means to enhance efficacy (yet, likely enhancing toxicity as well). These data also support the temporal pH data (Figures 6E and 6F), and together imply that Glycofект utilizes an active transport mechanism at later time points post-transfection.

Taken together, data in this study support our hypothesis that active transport of nucleic acids occurs

within the cell, utilizing the innate sorting and packaging organelles designed for shuttling proteins, over the time course of the nucleic acid delivery experiments. These data are corroborated by the observation that labeled ODNs are co-localized with organelles such as the Golgi, ER, and trafficking vesicles such as COPI, clathrin-coated pits, and caveolae 24 h after the initial cellular exposure to polyplexes. As mentioned, the cytoplasm is a perilous and crowded environment that would likely hinder the passive diffusion of nucleic acids within this environment and into the nucleus. In addition, these data also reveal that the biodegradable glycopolymers vehicle, Glycofект, undergoes different kinetics of intracellular trafficking, which possibly promotes delivery to a larger degree through this active trafficking route.

As previously mentioned, saccharide residues are well known for various signaling/routing events in biological systems, and the galactose residues in Glycofект could play a role in mediating the active transport of the polyplexes. For example, galectins, a class of carbohydrate-binding proteins, are well known to initiate signaling events regulating proliferation, apoptosis, and intracellular export.<sup>100,101</sup> Some studies have even revealed nuclear trafficking of galectin-3.<sup>102</sup> Previous studies on glycosylated polymers indicate that many carbohydrate moieties strongly affect intracellular routing; for example, mannosylated polyplexes appeared to stay longer in endosomes and accumulate in lysosomes more than lactosylated polyplexes.<sup>42,103,104</sup> Therefore, it is possible that Glycofект polyplexes are targeted to specialized organelles, such as the ER and Golgi, by virtue of their galactose moiety. Furthermore, because other glycosylated macromolecules, such as hormone receptors, have been shown to be transported from the ER to the nucleus, glycosylated NA delivery vehicles may also be able to exploit this pathway. Therefore, future efforts to tailor carbohydrate-containing vehicles to further exploit this active route toward the genetic center of a cell may greatly increase the efficacy of these nonviral nucleic acid delivery vehicles. This pathway is further supported by findings from a recent study with the PEI polymer: grafting with trimethylated and unmethylated histone H3 nuclear co-localization signal resulted in rapid accumulation of polyplexes in ER as early as 5 min post-transfection and gradually increased over 30 min, as compared to a low level of accumulation with native PEI.<sup>45</sup> Thus, the design of polymer structure is crucial for delineating the trafficking route toward an intracellular target. In addition, it should be noted that this trafficking behavior of Golgi and ER mimics viruses, such as Simian virus 40, polio-virus, and hepatitis C virus.<sup>105–110</sup>

## CONCLUSION

The primary finding of this study is that the structure of the polymer used to design a nonviral nucleic acid

delivery vehicle plays a vital role in its intracellular trafficking. Both linear PEI and Glycofect delivery vehicles promote alternative active transport routes en route to the nucleus, rather than just mediated *via* the “proton sponge effect”. The unique saccharide-based structure of Glycofect allows it to initiate cellular entry *via* various routes including caveolae, clathrin, macropinocytosis, and perhaps other less-characterized internalization routes. After cellular internalization, both linear PEI and Glycofect polyplexes can hitchhike *via* intracellular transport machinery, which leads to sorting to the Golgi and likely retrograde transport to the endoplasmic reticulum. While linear PEI polyplexes appear to localize to acidic endocytic vesicles, Glycofect

polyplexes appear to bypass lysosomes (more so than linear PEI) and appear to be, at least in part, trafficked through the Golgi and ER (corroborated by the high colocalization data of pDNA delivered by Glycofect) more so than PEI. We hypothesize that this active transport pathway ultimately aids or even leads to delivery to the nucleus and perhaps is the cause of more sustained gene expression kinetics of this delivery vehicle. Indeed, polymeric nucleic acid delivery vehicles appear to mediate delivery, at least in part, *via* pathways similar to viruses. Understanding how the structure of these vehicles impacts transport pathways will aid in the *de novo* design of more effective vehicles for specific applications.

## MATERIALS AND METHODS

**Materials.** Unless otherwise noted, all chemicals and reagents were purchased from Sigma-Aldrich (St. Louis, MO, USA). Glycofect (G4) was synthesized according to previously published procedures ( $M_w = 4.6$  kDa; degree of polymerization,  $n = 11$ ) and was used at an N/P ratio = 20 due to previous findings that higher N/P ratios promoted the highest transfection efficiency without cytotoxicity.<sup>11</sup> The polyplex sizes that are formed have been found to be around 110 nm, and the zeta potential has been found to be around 10 mV. Linear PEI ( $M_w \approx 22$  kDa) used in titrations was purchased from Polysciences, Inc. (Warrington, PA, USA). JetPEI (linear PEI,  $M_w = 22$  kDa) used in cell culture studies (N/P ratio = 5, recommended from the manufacturer) was purchased from Polyplus Transfection (New York, NY, USA). All primary antibodies were purchased from Abcam (Cambridge, MA, USA): clathrin, rabbit polyclonal antibody to clathrin heavy chain; caveolin, rabbit polyclonal antibody to caveolin-1; Golgi, mouse monoclonal antibody giantin; ER, rabbit polyclonal antibody to GRP78 BiP (ER lumen); COP I, rabbit polyclonal to beta COP. The secondary antibody (goat anti-rabbit IgG antibody labeled with Alexa Fluor 555 Dye) was purchased from Molecular Probes (Eugene, OR, USA).

**Cell Culture.** The H9c2(2-1) cell line was purchased from American Type Cell Culture Collection (ATCC, Rockville, MD, USA) and consists of cardiac-like myoblasts derived from BD1X rat myocardium. Cells were cultured under conditions recommended by ATCC. All cell culture media, antibiotic/antimycotic, fetal bovine serum (FBS), phosphate-buffered saline (PBS), and nuclease-free water were purchased from Gibco (Carlsbad, CA, USA). Plasmid DNA gWiz-Luc (6.7 kb) and pCMV-βGal (8.5 kb) were purchased from Aldevron Fargo (Fargo, ND, USA).

**Time-Course Transfection Efficiency Assay.** H9c2(2-1) cells were seeded into 24-well plates (Corning, MA, USA) at a density of 40,000 cells/well and cultured for 24 h at 37 °C and 5% CO<sub>2</sub>. One hour before transfection, polyplexes were formulated at the appropriate N/P ratio, where “N” is the number of secondary amines on the polymer and “P” is the number of phosphates on the plasmid DNA. The N/P ratios selected for polymers linear PEI and Glycofect were 5 and 20, respectively. To make polyplexes 50 μL/well of polymer solution was added to 50 μL/well of gWiz-Luc plasmid DNA (6.7 kb) solution at 0.02 μg/μL and mixed with gentle pipetting to make 100 μL/well polyplex solution. At the time of transfection, media was removed and the cells were washed with PBS (Gibco, Invitrogen, Carlsbad, CA, USA). Cells were transfected with 100 μL/well of polyplex solution in 200 μL/well of Opti-MEM (1 μg of plasmid DNA per well) and returned to the incubator at 37 °C and 5% CO<sub>2</sub>. All transfections were performed in triplicate and included negative controls of both untransfected cells and cells transfected with naked plasmid DNA. After 4 h, the Opti-MEM (reduced serum media) solution was aspirated and exchanged with Dulbecco's minimum essential medium (D-MEM) supplemented with 10% FBS,

100 units/mg penicillin, 100 μg/mL streptomycin, and 0.25 μg/mL amphotericin (Gibco, Invitrogen). At the appropriate time point, the cells were removed from the incubator, washed with PBS, and lysed with 100 μL/well of 1× lysis buffer (Promega, WI, USA). The amount of protein in each sample well was analyzed using a Bio-Rad DC protein assay kit (Hercules, CA, USA) and determined using a standard curve created with bovine serum albumin dissolved in cell lysis buffer. Lysates were also assayed for reporter gene activity using a luciferase assay kit (Promega). Luminescence was measured in duplicate over 10 s with a Tecan GENios Pro luminometer (Tecan US, Inc., Durham, NC, USA) and averaged for each sample. Cell viability is reported as the average amount of protein in cell lysates normalized against a control of untreated cells. The transfection efficiency of each vector is reported as relative light units (RLU)/mg of protein for each triplicate normalized against a control of plasmid DNA only.

**Oligonucleotide Synthesis and Annealing.** Two strands of 20 bp DNA oligonucleotide were synthesized *via* standard phosphoramidite chemistry. The sense strand sequence was 5' CCTTGAAGGGATTCCCTCC 3', and the antisense strand sequence was 5' GGAGGGAAATCCCTTAAGG 3'. Both oligos were phosphorothiolated completely and fluorescently labeled with FITC (sense strand) and/or Cy5 (antisense strand) at the 5' end. To anneal, the two oligos were dissolved in nuclease-free water and diluted to a concentration of 1 μg/μL in annealing buffer [0.05 M NaCl, 10 mM EDTA (ethylenediaminetetraacetic acid), 10 mM Tris pH 7.5]. The solution was then immersed in an 80 °C water bath for 10–15 min and then slowly allowed to recover to room temperature over the course of several hours.

**Buffering Capacity.** The protocol for titration of polymer solutions was slightly modified from a previously published method.<sup>20</sup> Briefly, the polymers were dissolved in PBS (pH 7.4) and the concentration of secondary amines was held constant at 0.7744 M for both polymer solutions. This concentration was chosen in an attempt to model the physiological concentration of polymer in endosomes during intracellular trafficking (assuming 1 polyplex, formulated with N/P = 15, and containing 1 plasmid DNA internalized by an endosome approximately 200 nm in diameter). Polymer solutions were titrated with 0.1 M standard HCl, and pH was monitored using an Accumet Basic AB15 pH meter (Pittsburgh, PA, USA). The titration data were analyzed *via* nonlinear regression using GraphPad Prism 4.0 (San Diego, CA, USA).

**Intracellular pH Assay.** H9c2(2-1) cells were seeded in six-well plates at a density of 200,000 cells/well in D-MEM containing 10% FBS, 100 units/mg penicillin, 100 μg/mL streptomycin, and 0.25 μg/mL amphotericin and cultured for 24 h before transfection. A few hours before transfection, polyplexes were formulated at N/P = 5 for PEI and N/P = 20 for Glycofect by adding polymer solution to annealed FITC-Cy5-labeled oligonucleotides (0.02 μg/μL); polyplexes were allowed to form for at least 1 h. At the time of transfection, D-MEM was aspirated, cells were

washed with PBS, and 1 mL of Opti-MEM was added to each well. Then 500  $\mu$ L of polyplex solution (5  $\mu$ g of DNA) was immediately added to each well, and the plates were swirled to evenly distribute the DNA and replaced in the incubator. After 4 h, the Opti-MEM solution was aspirated, the cells were washed extensively with PBS three times, and 2 mL of D-MEM was added to each well. The cells were returned to the incubator to allow DNA to traffic for the necessary amount of time (measurements taken at 8 and 24 h post-transfection). D-MEM was removed, and cells were again washed with PBS. The cells were trypsinized at 37 °C for 10–15 min and pelleted in an amber 1.5 mL Eppendorf tube. The cells were washed again in PBS and repelleted. Supernatant was removed, and cells were resuspended in either PBS or one of four pH clamping buffers (130 mM KCl, 1 mM MgCl<sub>2</sub>, 15 mM HEPES, and 15 mM MES), with pH adjusted to 4.02, 5.06, 5.51, 6.02, or 7.41 with dilute solutions of NaOH or HCl. The buffers were sterilized by filtration through a 0.2  $\mu$ m syringe filter. In indicated experiments, the buffers were supplemented with ionophores (0.010 mM valinomycin and 0.010 mM nigericin; Fluka, Sigma-Aldrich) and 200 nM baflomycin. The cells were then transferred to Falcon tubes and kept on ice until analyzed via flow cytometry on a FACS-Canto II (BD Biosciences, San Jose, CA, USA). At least 20,000 cells were measured in each sample. A negative control of untransfected cells was used to gate the level of positive fluorescence such that 1% or less of the untransfected cells was positive for either FITC or Cy5 fluorescence.

**Confocal Time-Course Microscopy.** H9c2(2-1) cells were seeded into six-well plates containing a 25 mm No. 1 coverslip at a density of 15,000 cells/well in supplemented DMEM (10% FBS, 100 units/mg penicillin, 100  $\mu$ g/mL streptomycin, and 0.25  $\mu$ g/mL amphotericin). Cells were cultured for 2 days to allow them to attach to coverslips. One hour before transfection, polyplexes were formulated by adding a solution of polymer to a solution of FITC-labeled annealed oligonucleotide at an N/P ratio of 5 for JetPEI and 20 for Glycofect (G4). At the time of transfection, media was removed from wells and cells were washed with PBS. Cells were transfected with 200  $\mu$ L of polyplex solution (2  $\mu$ g of oligonucleotide) in 2 mL of Opti-MEM and returned to the incubator. After 4 h, 2 mL of supplemented D-MEM was added to each well. Thirty minutes before the indicated time points, cells were removed from the incubator. Media was removed from each well, cells were washed twice with 2 mL of PBS, and 2 mL of 0.1  $\mu$ M Lysotracker Red (Molecular Probes) in supplemented D-MEM was added to each well. Cells were returned to the incubator for 30 min. Afterward, media was removed from cells, washed again with PBS, and fixed with 1% paraformaldehyde solution overnight. Before imaging, nuclei of cells were counterstained with DRAQ5 (Biostatus Limited, Leicestershire, UK) and mounted in ProLong Gold Antifade Reagent mounting media (Molecular Probes). Cells were imaged on a Zeiss LSM510 confocal system (Zeiss, Thornwood, NY, USA) fitted onto an Axioplan 2 upright microscope (Zeiss). Images were collected using the appropriate laser excitation and filter sets (FITC: excitation 488 nm and emission BP 505–550 nm; Lysotracker Red: excitation 543 nm, emission BP 560–615 nm; DRAQ5: excitation 633 nm, emission LP 650). Cells imaged were chosen based on being representative of the entire population observed. The confocal pinhole was opened to 1.5  $\mu$ m for all channels in order to capture the cytoplasmic distribution of DNA throughout the cells. In addition, DIC images were captured on a fourth channel to depict the morphology of transfected cells. Images were enhanced for brightness and contrast using ImageJ analysis software (National Institutes of Health, Bethesda, MD).<sup>111</sup>

**Endocytic Inhibition Experiments.** H9c2(2-1) cells were seeded at 200,000 cells/well in supplemented D-MEM (10% FBS, 100 units/mg penicillin, 100  $\mu$ g/mL streptomycin, and 0.25  $\mu$ g/mL amphotericin) in six-well tissue culture plates (Corning; Corning, NY, USA) and incubated for 24 h at 37 °C and 5% CO<sub>2</sub>. Polyplexes were formed with Cy5-labeled ODN as described above. Media was removed from the wells, and the cells were rinsed with PBS. Opti-MEM containing 2  $\mu$ g/mL cytochalasin D, chlorpromazine at 10  $\mu$ g/mL, and filipin III at 1  $\mu$ g/mL (2 mL) was added to each well. Plates were returned to the incubator, and cells were preincubated with the drugs for the amount of time indicated (Figure S5). Polyplex solution (300  $\mu$ L) was added directly to

each well and swirled to mix. Negative controls were treated with 300  $\mu$ L of Opti-MEM ("cells only") or uncomplexed plasmid DNA ("DNA only"). Cells were allowed to transfect for 2 h at 37 °C and 5% CO<sub>2</sub>. After 2 h, 3 mL of supplemented D-MEM was added to each well, and cells were incubated an additional 30 min. After removing the media and rinsing with PBS, 500  $\mu$ L of Trypsin-EDTA was added to each well and the cells were incubated until detached from the well (5–10 min). D-MEM containing 10% FBS (1 mL) was added to inactivate trypsin, and the contents of each well were transferred to a Falcon Tube (BD Biosciences). Cells were centrifuged at 4 °C and 1000 rpm for 10 min, then resuspended in 2% FBS in PBS. Cellular uptake was measured on a BD FACSCanto II Flow Cytometer (BD Biosciences). Propidium iodide (PI) was added to each tube at a concentration of 5  $\mu$ g/mL and volume 2.5  $\mu$ L/tube, and the tubes were gently vortexed 2–5 min prior to analysis. Appropriate gating was performed using a negative control (untreated H9c2(2-1) cells) to ensure that autofluorescent and PI-positive cells were excluded from subsequent analysis. Compiled data are an average of at least two replications (with the exception of caveolae inhibition, which was a single experiment). Cy5 was excited using a 633 nm helium-neon laser and detected with a 660/20 nm emission bandpass filter; propidium iodide was excited with a 488 nm solid-state laser, and fluorescence emission was detected by a 670 nm long-pass filter. A total of 10,000–20,000 gated events were collected for each sample. Data analysis was done using BD FACSDiva software (BD Biosciences).

**Immunocytochemistry.** H9c2(2-1) cells were seeded into 12-well plates containing a 15 mm No. 1 coverslip at a density of 12,000 cells/well and incubated at 37 °C under a 5% CO<sub>2</sub> atmosphere for 24 h prior to transfection. Polyplexes were formed by adding 50  $\mu$ L of 0.02  $\mu$ g/ $\mu$ L FITC-labeled annealed ODN to 50  $\mu$ L of polymer solution diluted to the appropriate concentration to reach N/P = 5 (JetPEI) or N/P = 20 (Glycofect). After incubation for 1 h at room temperature, cells were aspirated of media, washed with 0.5 mL of PBS, and transfected with 400 mL of Opti-MEM/polyplex solution (corresponding to 1  $\mu$ g of plasmid DNA/well). Cells were allowed to incubate at 37 °C under a 5% CO<sub>2</sub> atmosphere for 4 h, and then 930  $\mu$ L of fully supplemented D-MEM was added to each well. After an additional 20 h incubation, cells were aspirated of media and washed three times with 1 mL of PBS. One milliliter of 1% PFA (paraformaldehyde) in PBS was added to each well, and the cells were stored at 4 °C overnight. PFA was aspirated from each well, and cells were washed three times with 1 mL of PBS. Cells were then incubated at room temperature with 0.25% Triton X-100 (Integra Chemical Co., Kent, WA, USA) for 10 min and then washed with 1 mL of PBS for 5 min. Cells were blocked in a solution of 1% BSA in PBS at room temperature for 40 min. Afterward, BSA solution was removed from each well and 500  $\mu$ L of the specified primary antibody dissolved in 1% BSA in PBS solution was added to each well and allowed to incubate at room temperature for 1 h. (Concentrations used: clathrin, 1  $\mu$ g/mL; caveolin, 1/500 dilution of provided manufacturer solution; Golgi, 2  $\mu$ g/mL; ER, 1  $\mu$ g/mL; COP1, 1/2000 dilution of the provided manufacturer solution.) Afterward, the primary antibody solution was removed from each well and cells were washed three times with 1 mL of PBS for 5 min. Coverslips were then carefully placed cell-side down into 100  $\mu$ L of 5  $\mu$ g/mL secondary antibody solution in a humidified chamber and allowed to incubate for an additional hour. Afterward, cells were again washed three times with 1 mL of PBS for five times and placed cell-side down into 50  $\mu$ L of DRAQ5 (Biostatus Limited) nuclear counterstain solution (10  $\mu$ M) and allowed to incubate at room temperature for 5–10 min. Coverslips were carefully removed from DRAQ5 solution and washed with 1 mL of PBS before being mounted in ProLong Gold Antifade Reagent (Molecular Probes).

Cells were imaged on a LSM510 confocal system (Zeiss) fitted onto an Axioplan 2 upright microscope (Zeiss). Images were collected using the appropriate laser excitation and filter sets (FITC: excitation 488 nm and emission BP 505–550 nm; Alexa Fluor555 dye: excitation 543 nm and emission BP 560–615; DRAQ5: excitation 633 nm, emission LP 650). The cells depicted in all figures were chosen based on being representative

of the entire population observed. The confocal pinhole was opened to capture a vertical optical slice of  $0.8\text{ }\mu\text{m}$  in all channels. Images were initially processed using the despeckle algorithm (through ImageJ),<sup>111</sup> and then appropriate background subtraction was applied to each image. Images were then minimally processed for brightness and contrast enhancement using ImageJ. Co-localization highlighting was also processed using the Colocalization Highlighter plugin for ImageJ. Manders' coefficient<sup>88</sup> ( $M_1$ , for green (ODN) pixels overlapping red (ER) pixels) was calculated using the JACoP plug-in<sup>112</sup> for ImageJ<sup>111</sup> as shown in eq 1. Manders' coefficient ranges from 0 to 1, where 1 denotes complete co-localization and 0 represents none:

$$M_1 = \frac{\sum_i G_{i,\text{co-loc}}}{\sum_i G_i} \quad (1)$$

where  $G_{i,\text{co-loc}}$  is the intensity of green pixels overlapping red pixels and  $G_i$  is the total intensity of green pixels.

**Confocal Live Cell Imaging.** H9c2(2-1) cells were seeded into six-well plates containing a 25 mm No. 1 coverslip (Mattek Corporation) at a density of 12,000 cells/well. Cells were allowed to culture for 24 h before transfection. A few hours before transfection, polyplexes were formulated by adding a solution of polymer to a solution of double-labeled (FITC-Cy5) annealed oligonucleotide at an N/P ratio of 5 for JetPEI and 20 for Glycofect. At the time of transfection, media was removed from wells and cells were washed with PBS. Cells were transfected with 200  $\mu\text{L}$  of polyplex solution (2  $\mu\text{g}$  of oligonucleotide) in 2 mL of Opti-MEM and returned to the incubator. For cells allowed to transfect for 30 h, after the initial 4 h of transfection, 2 mL of supplemented D-MEM was added to each well. Live cells were imaged on an LSM10 confocal system (Zeiss, Thornwood, NY) fitted onto an Zeiss Axiovert 100 M inverted microscope with recessed incubated stage. Images were collected using the appropriate laser excitation and filter sets (FITC: excitation 488 nm and emission BP 505–550; Cy5: excitation 633 nm and emission LP 650). Cells imaged were chosen based on being representative of the entire population observed. Images were enhanced for brightness and contrast using ImageJ analysis software.<sup>111</sup>

**Live Cell Time-Lapse Image Processing.** Images were initially processed using the despeckle algorithm (through ImageJ), and then appropriate background subtraction was applied to each image. In some cases an FFT bandpass or Kalman filter was used to increase the clarity of the presented images; however, all ratio calculations were performed on images prior to applying these filters.

**Ratio Calculations of Live Cell Time-Lapse Images.** A cell to be analyzed was cropped out of the original image, and FITC and Cy5 brightness and contrast were adjusted simultaneously in a merged image. The pixels representing intracellular plasmid DNA to be analyzed were subjected to threshold, and background (black) pixels were converted to “not a number” to remove them from the calculation. The mean pixel intensity of FITC and Cy5 in each cell at each time point in the time series was then measured separately. Dividing the mean FITC pixel intensity by the mean Cy5 pixel intensity and plotting this ratio against the corresponding time point produced the intracellular pH graphs depicted in Figure 6E, F.

**Acridine Orange Assay.** H9c2(2-1) cells were seeded in six-well cell culture plates at a density of 100,000 cells/well. A lower number of cells was used to reduce cell-to-cell confluence at extended time points in the experiments. The polyplexes were formulated by adding 125  $\mu\text{L}$  of polymer to 125  $\mu\text{L}$  of NFkB oligonucleotide in DNase RNase-free H<sub>2</sub>O and incubated for 1 h at room temperature. Prior to transfection, the polyplexes were diluted in 500  $\mu\text{L}$  of Opti-MEM. The transfected cells were incubated at 37 °C for 15 min. After 4 h, 1 mL of DMEM was added to each well. Later, at time points 4, 8, 12, 16, 20, and 24 h, the cells were treated with 5  $\mu\text{g}/\text{mL}$  of AO solution in D-MEM at 37 °C for 15 min and then prepared for flow cytometry experiment. The lysosomal fluorescence due to AO was measured on a FACS Cantoll flow cytometer (BD Biosciences) for 20,000 cells. The 488 nm argon laser was used to excite red lysosomal fluorescence and detected at 670 nm. The FACSDiva software (BD Biosciences) was used to acquire data. The loss in detected

fluorescence was attributed to rupture of lysosomes, causing a reduction in intensity. These cells were referred to as “pale cells”.

**Conflict of Interest:** The authors declare the following competing financial interest(s): T.M.R. is a consultant to and has stock options in Techulon, Inc.

**Supporting Information Available:** Figures S1–S6 and Movies S1 to S4. This material is available free of charge via the Internet at <http://pubs.acs.org>.

**Acknowledgment.** The authors wish to thank NIH 1-R21-EB3938-01 and the Director's New Innovator Award program (DP2-OD006669-01) for funding of this project.

## REFERENCES AND NOTES

- Opalinksak, J. B.; Gewirtz, A. M. Nucleic-Acid Therapeutics: Basic Principles and Recent Applications. *Nat. Rev. Drug Discovery* **2002**, *1*, 503–514.
- Breaker, R. R. Natural and Engineered Nucleic Acids as Tools to Explore Biology. *Nature* **2004**, *423*, 838–845.
- Davis, M. E.; Brewster, M. E. Cyclodextrin-Based Pharmaceuticals: Past, Present and Future. *Nat. Rev. Drug Discovery* **2004**, *3*, 1023–1035.
- Davis, M. E.; Zuckerman, J. E.; Choi, C. H. J.; Seligson, D.; Tolcher, A.; Alabi, C. A.; Yen, Y.; Heidel, J. D.; Ribas, A. Evidence of RNAi in Humans from Systemically Administered siRNA via Targeted Nanoparticles. *Nature* **2010**, *464*, 1067–1070.
- Gaudet, D.; de Wal, J.; Tremblay, K.; Déry, S.; van Deventer, S.; Freidig, A.; Brisson, D.; Méthot, J. Review of the Clinical Development of Alipogene Tiparvovec Gene Therapy for Lipoprotein Lipase Deficiency. *Atheroscler. Suppl.* **2010**, *11*, 55–60.
- Ingle, N. P.; Malone, B.; Reineke, T. M. Poly(glycoamidoamine)s: A Broad Class of Carbohydrate-Containing Polycations for Nucleic Acid Delivery. *Trends Biotechnol.* **2011**, *29*, 443–453.
- Kay, M. A.; Glorioso, J. C.; Naldini, L. Viral Vectors for Gene Therapy: the Art of Turning Infectious Agents into Vehicles of Therapeutics. *Nat. Med.* **2001**, *7*, 33–40.
- Zimmermann, T. S.; Lee, A. C. H.; Akinc, A.; Bramlage, B.; Bumcrot, D.; Fedoruk, M. N.; Harborth, J.; Heyes, J. A.; Jeffs, L. B.; John, M.; et al. RNAi-Mediated Gene Silencing in Non-Human Primates. *Nature* **2006**, *441*, 111–114.
- Hrkach, J.; Von Hoff, D.; Ali, M. M.; Andrianova, E.; Auer, J.; Campbell, T.; De Witt, D.; Figa, M.; Figueiredo, M.; Horhota, A.; et al. Preclinical Development and Clinical Translation of a PSMA-Targeted Docetaxel Nanoparticle with a Differentiated Pharmacological Profile. *Sci. Transl. Med.* **2012**, *4*, 1–11.
- Boussif, O.; Lezoualc'h, F.; Zanta, M. A.; Mergny, M. D.; Scherman, D.; Demeneix, B.; Behr, J. P. A Versatile Vector for Gene and Oligonucleotide Transfer into Cells in Culture and *in Vivo*: Polyethylenimine. *Proc. Natl. Acad. Sci. U. S. A.* **1995**, *92*, 7297–7301.
- Liu, Y.; Reineke, T. M. Hydroxyl Stereochemistry and Amine Number within Poly(glycoamidoamine)s Affect Intracellular DNA Delivery. *J. Am. Chem. Soc.* **2005**, *127*, 3004–3015.
- Srinivasachari, S.; Fichter, K. M.; Reineke, T. M. Polycationic  $\beta$ -Cyclodextrin “Click Clusters”: Monodisperse and Versatile Scaffolds for Nucleic Acid Delivery. *J. Am. Chem. Soc.* **2008**, *130*, 4618–4627.
- Fichter, K. M.; Zhang, L.; Kiick, K. L.; Reineke, T. M. Peptide-Functionalized Poly(ethylene glycol) Star Polymers: DNA Delivery Vehicles with Multivalent Molecular Architecture. *Bioconjugate Chem.* **2008**, *19*, 76–88.
- Harada, A.; Kawamura, M.; Matsuo, T.; Toshinari, T.; Kono, K. Synthesis and Characterization of a Head-Tail type Polycation Block Copolymer as a Nonviral Gene Vector. *Bioconjugate Chem.* **2006**, *17*, 3–5.
- Shuai, X.; Merdan, T.; Unger, F.; Kissel, T. Supromolecular Gene Delivery Vectors Showing Enhanced Trans-Gene

- Expression and Good Biocompatibility. *Bioconjugate Chem.* **2005**, *16*, 322–329.
16. Anderson, D. G.; Akinc, A.; Hossain, N.; Langer, R. Structure/Property Studies of Polymeric Gene Delivery Using a Library of Poly( $\beta$ -amino esters). *Mol. Ther.* **2005**, *11*, 426–434.
  17. Reineke, T. M.; Davis, M. E. Structural Effects of Carbohydrate-Containing Polycations on Gene Delivery. 1. Carbohydrate Size and Its Distance from Charged Centers. *Bioconjugate Chem.* **2003**, *14*, 247–254.
  18. Reineke, T. M.; Davis, M. E. Structural Effects of Carbohydrate-Containing Polycations on Gene Delivery. 2. Charge Center Type. *Bioconjugate Chem.* **2003**, *14*, 255–261.
  19. Popielarski, S. R.; Mishra, S.; Davis, M. E. Structural Effects of Carbohydrate-Containing Polycations on Gene Delivery. 3. Cyclodextrin Type and Functionalization. *Bioconjugate Chem.* **2003**, No.), 672–678.
  20. Liu, Y.; Reineke, T. M. Poly(glycoamidoamine)s for Gene Delivery. Structural Effects on Cellular Internalization, Buffering Capacity, and Gene Expression. *Bioconjugate Chem.* **2007**, *18*, 19–30.
  21. Zelphati, O.; Szoka, F. C., Jr. Mechanism of Oligonucleotide Release from Cationic Liposomes. *Proc. Natl. Acad. Sci. U. S. A.* **1996**, *93*, 11493–11498.
  22. Lewis, J. G.; Lin, K. Y.; Kothavale, A.; Flanagan, W. M.; Matteucci, M. D.; DePrince, R. B.; Mook, R. A., Jr.; Hendren, R. W.; Wagner, R. W. A Serum-Resistant Cytofectin for Cellular Delivery of Antisense Oligodeoxynucleotides and Plasmid DNA. *Proc. Natl. Acad. Sci. U. S. A.* **1996**, *93*, 3176–3181.
  23. Mishra, S.; Heidel, J. D.; Webster, P.; Davis, M. E. Imidazole Groups on a Linear, Cyclodextrin-Containing Polycation Produce Enhanced Gene Delivery via Multiple Processes. *J. Controlled Release* **2006**, *116*, 179–191.
  24. Elouahabi, A.; Ruysscharet, J.-M. Formation and Intracellular Trafficking of Lipoplexes and Polyplexes. *Mol. Ther.* **2005**, *11*, 336–347.
  25. Goncalves, C.; Mennesson, E.; Ruchs, R.; Gorvel, J.-P.; Midoux, P.; Pichon, C. Macropinocytosis of Polyplexes and Recycling of Plasmid via the Clathrin-Dependant Pathway Impare the Transfection Efficiency of Human Hepatocarcinoma Cells. *Mol. Ther.* **2004**, *10*, 373–385.
  26. Rejman, J.; Bragonzi, A.; Conese, M. Role of Clathrin- and Caveolae-Mediated Endocytosis in Gene Transfer Mediated by Lipo- and Polyplexes. *Mol. Ther.* **2005**, *12*, 468–474.
  27. Manunta, M.; Nichols, B. J.; Tan, P. H.; Sagoo, P.; Harper, J.; George, A. J. Gene Delivery by Dendrimers Operates via Different Pathways in Different Cells, but is Enhanced by the Presence of Caveolin. *J. Immunol. Methods* **2006**, *314*, 134–146.
  28. Grosse, S.; Aron, Y.; Thevenot, G.; Francois, D.; Monsigny, M.; Fajac, I. Potocytosis and Cellular Exit of Complexes as Cellular Pathways for Gene Delivery by Polycations. *J. Gene Med.* **2005**, *7*, 1275–1286.
  29. Forrest, M. L.; Pack, D. W. On the Kinetics of Polyplex Endocytic Trafficking: Implications for Gene Delivery Vector Design. *Mol. Ther.* **2002**, *6*, 57–65.
  30. Plank, C.; Oberhauser, B.; Mechtler, K.; Koch, C.; Wagner, E. The Influence of Endosome-Disruptive Peptides on Gene Transfer Using Synthetic Virus-like Gene Transfer Systems. *J. Biol. Chem.* **1994**, *269*, 12918–24.
  31. Ogris, M.; Carlisle, R. C.; Bettinger, T.; Seymour, L. W. Melittin Enables Efficient Vesicular Escape and Enhanced Nuclear Access of Nonviral Gene Delivery Vectors. *J. Biol. Chem.* **2001**, *276*, 47550–47555.
  32. Haensler, J.; Szoka, F. C. Polyamidoamine Cascade Polymers Mediate Efficient Transfection of Cells in Culture. *Bioconjugate Chem.* **1993**, *4*, 372–379.
  33. Putnam, D.; Gentry, C. A.; Pack, D. W.; Langer, R. Polymer-Based Gene Delivery with Low Cytotoxicity by a Unique Balance of Side-Chain Termini. *Proc. Natl. Acad. Sci. U. S. A.* **2001**, *98*, 1200–1205.
  34. Nel, A. E.; Madler, L.; Velegol, D.; Xia, T.; Hoek, E. M. V.; Somasundaran, P.; Klaessig, F.; Castranova, V.; Thompson, M. Understanding Biophysicochemical Interactions at the Nano-Bio Interface. *Nat. Mater.* **2009**, *8*, 543–557.
  35. Grandinetti, G.; Ingle, N. P.; Reineke, T. M. Interaction of Poly(ethylenimine)-DNA Polyplexes with Mitochondria: Implications for a Mechanism of Cytotoxicity. *Mol. Pharm.* **2011**, *8*, 1709–1719.
  36. Lechardeur, D.; Lukacs, G. L. Nucleocytoplasmic Transport of Plasmid DNA: A Perilous Journey from the Cytoplasm to the Nucleus. *Hum. Gene Ther.* **2006**, *9*, 882–889.
  37. Lechardeur, D.; Drzymala, L.; Sharma, M.; Zylka, D.; Kinach, R.; Pacia, J.; Hicks, C.; Usmani, N.; Rommens, J. M.; Lukacs, G. L. Determinants of the Nuclear Localization of the Heterodimeric DNA Fragmentation Factor (Icad/Cad). *J. Cell Biol.* **2000**, *150*, 321–334.
  38. Lechardeur, D.; Lukacs, G. L. Intracellular Barriers to Non-Viral Gene Transfer. *Curr. Gene Ther.* **2002**, *2*, 183–194.
  39. Rejman, J.; Bragonzi, A.; Conese, M. Role the Cathrin- and Caveolae-Mediated Endocytosis in Gene Transfer Mediated by Lipo- and Polyplexes. *Mol. Ther.* **2005**, *12*, 468–474.
  40. von Gersdoff, K.; Sanders, N. N.; Vandenbroucke, R.; De Smedt, S. D.; Wagner, E.; Ogris, M. The Internalization Route Resulting in Successful Gene Expression Depends on both Cell Line and Polyethylenimine Polyplex Type. *Mol. Ther.* **2006**, *14*, 745–753.
  41. Bieber, T.; Meissner, W.; Kostin, S.; Niemann, A.; Elsasser, H.-P. Intracellular Route and Transcriptional Competence of Polyethylenimine-DNA Complexes. *J. Controlled Release* **2002**, *82*, 441–454.
  42. Grosse, S.; Aron, Y.; Honore, I.; Thevenot, G.; Danel, C.; Roche, A.-C.; Monsigny, M.; Fajac, I. Lactosylated Polyethylenimine for Gene Transfer into Airway Epithelial Cells: Role of the Sugar Moiety in Cell Delivery and Intracellular Trafficking of the Complexes. *J. Gene Med.* **2004**, *2004*, 345–356.
  43. Godbey, W. T.; Wu, K. K.; Mikos, A. G. Tracking the Intracellular Path of Poly(ethylenimine)/DNA Complexes for Gene Delivery. *Proc. Natl. Acad. Sci. U. S. A.* **1999**, *96*, 5177–5181.
  44. Qi, R.; Mullen, D. G.; Baker, J. R.; Banaszak Holl, M. M. The Mechanism of Polyplex Internalization into Cells: Testing the GM1/Caveolin-1 Lipid Raft Mediated Endocytosis Pathway. *Mol. Pharmaceutics* **2009**, *7*, 267–279.
  45. Reilly, M. J.; Larsen, J. D.; Sullivan, M. O. Polyplexes Traffic through Caveolae to the Golgi and Endoplasmic Reticulum en Route to the Nucleus. *Mol. Pharm.* **2012**, *9*, 1280–1290.
  46. Grandinetti, G.; Reineke, T. M. Exploring the Mechanism of Plasmid DNA Nuclear Internalization with Polymer-Based Vehicles. *Mol. Pharm.* **2012**, *9*, 2256–2267.
  47. McLendon, P. M.; Fichter, K. M.; Reineke, T. M. Poly(glycoamidoamine) Vehicles Promote pDNA Uptake through Multiple Routes and Efficient Gene Expression via Caveolae-Mediated Endocytosis. *Mol. Pharmaceutics* **2010**, *7*, 738–750.
  48. Kim, H. H.; Lee, W. S.; Yang, J. M.; Shin, S. Basic Peptide System for Efficient Delivery of Foreign Genes. *Biochim. Biophys. Acta* **2003**, *1640*, 129–136.
  49. Ferrari, A.; Pellegrini, V.; Arcangeli, C.; Fittipaldi, A.; Giacca, M.; Beltram, F. Caveolae-Mediated Internalization of Extracellular HIV-1 tat Fusion Proteins Visualized in Real Time. *Mol. Ther.* **2003**, *8*, 284–294.
  50. Tagawa, A.; Mezzacasa, A.; Hayer, A.; Longatti, A.; Pelkmans, L.; Helenius, A. Assembly and Trafficking of Caveolar Domains in the Cell: Caveolae as Stable, Cargo-Triggered, Vesicular Transporters. *J. Cell. Biol.* **2005**, *170*, 769–779.
  51. Gabrielson, N. P.; Pack, D. W. Efficient Polyethylenimine-Mediated Gene Delivery Proceeds via a Caveolar Pathway in HeLa Cells. *J. Controlled Release* **2009**, *136*, 54–61.
  52. Lee, M. C.; Miller, E. A.; Goldberg, J.; Orci, L.; Schekman, R. Bi-directional Protein Transport between the ER and Golgi. *Annu. Rev. Cell Dev. Biol.* **2004**, *20*, 87–123.

53. Raykhel, I.; Alanen, H.; Salo, K.; Jurvansuu, J.; Nguyen, V. D.; Latva-Ranta, M.; Ruddock, L. A Molecular Specificity Code for the Three Mammalian KDEL Receptors. *J. Cell. Biol.* **2007**, *179*, 1193–1204.
54. Cosson, P.; Letourneur, F. Coatomer (COPI)-Coated Vesicles: Role in Intracellular Transport and Protein Sorting. *Curr. Opin. Cell. Biol.* **1997**, *9*, 484–487.
55. Lippincott-Schwartz, J. Bidirectional Membrane Traffic between the Endoplasmic Reticulum and Golgi Apparatus. *Trends Cell Biol.* **1993**, *3*, 81–88.
56. Levine, T.; Rabouille, C. Endoplasmic Reticulum: One Continuous Network Compartmentalized by Extrinsic Cues. *Curr. Opin. Cell. Biol.* **2005**, *4*, 362–368.
57. Liao, H.-J.; Carpenter, G. Role of the Sec61 Translocon in EGF Receptor Trafficking to the Nucleus and Gene Expression. *Mol. Biol. Cell* **2007**, *18*, 1064–1072.
58. Chen, T.-L. L. W., P. Y.; Luo, W.; Gwon, S. S.; Flay, N. W.; Zheng, J.; Guo, C.; Tanzer, M. L.; Vertel, B. M. Aggrecan Domains Expected to Traffic Through the Exocytic Pathway are Misdirected to the Nucleus. *Exp. Cell Res.* **2001**, *263*, 224–235.
59. Lv, H.; Zhang, S.; Wang, B.; Cui, S.; Yan, J. Toxicity of Cationic Lipids and Cationic Polymers in Gene Delivery. *J. Controlled Release* **2006**, *114*, 100–109.
60. Moghimi, S. M.; Symonds, P.; Murray, J. C.; Hunter, A. C.; Debska, G.; Szewczyk, A. A Two-Stage Poly(ethyleneimine)-Mediated Cytotoxicity: Implications for Gene Transfer/Therapy. *Mol. Ther.* **2005**, *11*, 990–995.
61. Florea, B. I.; Meaney, C.; Junginger, H. E.; Borchard, G. Transfection Efficiency and Toxicity of Polyethyleneimine in Differentiated Calu-3 and Nondifferentiated COS-1 Cell Cultures. *AAPS PharmSci* **2002**, *4*, 1–11.
62. Liu, Y.; Reineke, T. M. Poly(glycoamidoamine)s for Gene Delivery: Stability of Polyplexes and Efficacy with Cardiomyoblast Cells. *Bioconjugate Chem.* **2006**, *17*, 101–108.
63. Lee, C.-C.; Liu, Y.; Reineke, T. M. General Structure-Activity Relationship for Poly(glycoamidoamine)s: The Effect of Amine Density on Cytotoxicity and DNA Delivery Efficiency. *Bioconjugate Chem.* **2008**, *19*, 428–440.
64. Prevette, L. E.; Kodger, T. E.; Reineke, T. M.; Lynch, M. L. Deciphering the Role of Hydrogen Bonding in Enhancing pDNA-Polycation Interactions. *Langmuir* **2007**, *23*, 9773–9784.
65. Liu, Y.; Wenning, L.; Lynch, M.; Reineke, T. M. Gene Delivery with Novel Poly(l-tartaramidoamine)s. In *Polymeric Drug Delivery Vol. I - Particulate Drug Carriers*; Svenson, S., Ed.; American Chemical Society: Washington, D.C., 2005; pp 217–227.
66. Liu, Y.; Wenning, L.; Lynch, M.; Reineke, T. M. Now Poly-( $\omega$ -glucaramidoamine)s Induce DNA Nanoparticle Formation and Efficient Gene Delivery into Mammalian Cells. *J. Am. Chem. Soc.* **2004**, *126*, 7422–7423.
67. Liu, Y.; Reineke, T. M. Degradation of Poly(glycoamidoamine) DNA Delivery Vehicles: Polyamide Hydrolysis at Physiological Conditions Promotes DNA Release. *Biomacromolecules* **2010**, *11*, 316–325.
68. Akinc, A.; Thomas, M.; Klipanov, A. M.; Langer, R. Exploring polyethylenimine-mediated DNA Transfection and the Proton Sponge Hypothesis. *J. Gene Med.* **2005**, *7*, 657–663.
69. Akinc, A.; Langer, R. Measuring the pH Environment of DNA Delivered Using Nonviral Vectors: Implications for Lysosomal Trafficking. *Biotechnol. Bioeng.* **2002**, *78*, 503–508.
70. Crider, B. P.; Xie, X.-S.; Stones, D. K. Bafilomycin Inhibits Proton Flow through the  $H^+$  Channel of Vacuolar Proton Pumps. *J. Biol. Chem.* **1994**, *269*, 17379–17381.
71. Forgac, M. Structure and Properties of the Coated Vesicle ( $H^+$ )-ATPase. *J. Bioenerg. Biomembr.* **1992**, *24*, 341–350.
72. Hong, W.; Bielinska, A. U.; Mecke, A.; Keszler, B.; Beals, J. L.; Shi, X.; Balogh, L.; Orr, B. G.; Baker, J. R., Jr.; Banaszak Holl, M. M. Interaction of Poly(amidoamine) Dendrimers with Supported Lipid Bilayers and Cells: Hole Formation and the Relation to Transport. *Bioconjugate Chem.* **2004**, *15*, 774–782.
73. Hong, S.; Leroueil, P. R.; Janus, E. K.; Peters, J. L.; Kober, M.-M.; Islam, M. T.; Orr, B. G.; Baker, J. R., Jr.; Banaszak Holl, M. M. Interaction of Polycationic Polymers with Supported Lipid Bilayers and Cells: Nanoscale Hole Formation and Enhanced Membrane Permeability. *Bioconjugate Chem.* **2006**, *17*, 728–734.
74. Intra, J.; Salem, A. K. Fabrication, Characterization and *in Vitro* Evaluation of Poly(D,L-lactide-co-glycolide) Microparticles Loaded with Polyamidoamine–Plasmid DNA Dendriplexes for Applications in Nonviral Gene Delivery. *J. Pharm. Sci.* **2010**, *99*, 368–384.
75. Zhang, X.-Q.; Intra, J.; Salem, A. K. Conjugation of Polyamidoamine Dendrimers on Biodegradable Microparticles for Nonviral Gene Delivery. *Bioconjugate Chem.* **2007**, *18*, 2068–2076.
76. Caruso, J. A.; Mathieu, P. A.; Joakim, A.; Leeson, B.; Kessel, D.; Sloane, B. F.; Reiners, J. J. Differential Susceptibilities of Murine Hepatoma 1c1c7 and Tao Cells to the Lysosomal Photosensitizer NP6: Influence of Aryl Hydrocarbon Receptor on Lysosomal Fragility and Protease Contents. *Mol. Pharmacol.* **2004**, *65*, 1016–1028.
77. Girao, H.; Geli, M.-I.; Idrissi, F.-Z. Actin in the Endocytic Pathway: From Yeast to Mammals. *FEBS Lett.* **2008**, *582*, 2112–2119.
78. Pauly, B. S.; Drubin, D. G. Clathrin: An Amazing Multi-functional Dreamcoat? *Cell Host Microbe* **2007**, *2*, 288–290.
79. Pelkmans, L.; Helenius, A. Endocytosis via Caveolae. *Traffic* **2002**, *2*, 311–320.
80. Hewlett, L. J.; Prescott, A. R.; Watts, C. The Coated Pit and Macropinocytic Pathways Serve Distinct Endosome Populations. *J. Cell. Biol.* **1994**, *124*, 689–703.
81. Gonzalez-Gaitan, M.; Stenmark, H. Endocytosis and Signaling: A Relationship Under Development. *Cell* **2003**, *115*, 513–521.
82. Prentki, M.; Chaponnier, C.; Jeanrenaud, B.; Gabbiani, G. Actin Microfilaments, Cell Shape, and Secretory Processes in Isolated Rat Hepatocytes. Effect of Phalloidin and Cytochalasin D. *J. Cell Biol.* **1979**, *81*, 592–607.
83. McLendon, P. M.; Buckwalter, D. J.; Davis, E. M.; Reineke, T. M. Interaction of Poly(glycoamidoamine) DNA Delivery Vehicles with Cell-Surface Glycosaminoglycans Leads to Polyplex Internalization in a Manner Not Solely Dependent on Charge. *Mol. Pharmaceutics* **2010**, *7*, 1757–1768.
84. Yim, Y.-I.; Scarselletta, S.; Zang, F.; Wu, X.; Lee, D.; Kang, Y.; Eisenberg, E.; Greene, L. E. Exchange of Clathrin, AP2 and Epsin on Clathrin-Coated Pits in Permeabilized Tissue Culture Cells. *J. Cell. Sci.* **2005**, *118*, 2405–2413.
85. Seib, F. P.; Jones, A. T.; Duncan, R. Comparison of the Endocytic Properties of Linear and Branched PEIs, and Cationic PAMAM Dendrimers in B16f10 Melanoma Cells. *J. Controlled Release* **2007**, *117*, 291–300.
86. Llopis, J.; McCaffery, J. M.; Miyawaki, A.; Farquhar, M. G.; Tsien, R. Y. Measurement of Cytosolic, Mitochondrial, and Golgi pH in Single Living Cells with Green Fluorescent Proteins. *Proc. Natl. Acad. Sci. U. S. A.* **1998**, *95*, 6803–6808.
87. Seksek, O.; Biwersi, J.; Verkman, A. S. Direct Measurement of trans-Golgi pH in Living Cells and Regulation by Second Messengers. *J. Biol. Chem.* **1995**, *270*, 4967–4970.
88. Manders, E. M. M.; Stap, J.; Brakenhoff, G. J.; Van Driel, R.; Aten, A. Dynamics of Three-Dimensional Replication Patterns during the S-phase, Analysed by Double Labeling of DNA and Confocal Microscopy. *J. Cell Sci.* **1992**, *103*, 857–862.
89. Le, P. U.; Nabi, I. R. Distinct Caveolae-Mediated Endocytic Pathways Target the Golgi Apparatus and the Endoplasmic Reticulum. *J. Cell Sci.* **2003**, *116*, 1059–1071.
90. Geisow, M. J. Fluorescein Conjugates as Indicators of Subcellular pH: A Critical Evaluation. *Exp. Cell Res.* **1984**, *150*, 29–35.
91. Helander, I. M.; Alakomi, H. L.; Latva-Kala, K.; Koski, P. Polyethylenimine is an Effective Permeabilizer of Gram-Negative Bacteria. *Microbiology* **1997**, *143*, 3193–3199.

92. Klemm, A. R.; Young, D.; Lloyd, J. B. Effects of Polyethyleneimine on Endocytosis and Lysosome Stability. *Biochem. Pharmacol.* **1998**, *56*, 41–46.
93. Hunter, A. C.; Moghimi, S. M. Cationic Carriers of Genetic Material and Cell Death: A Mitochondrial Tale. *Biochim. Biophys. Acta* **2010**, *1797*, 1203–1209.
94. Funhoff, A. M.; van Nostrum, C. F.; Koning, G. A.; Schuurmans-Nieuwenbroek, N. M. E.; Crommelin, D. J. A.; Hennink, W. E. Endosomal Escape of Polymeric Gene Delivery Complexes Is Not Always Enhanced by Polymers Buffering at Low pH. *Biomacromolecules* **2004**, *5*, 32–39.
95. Forrest, M. L.; Meister, G. E.; Koerber, J. T.; Pack, D. W. Partial Acetylation of Polyethyleneimine Enhances *in Vitro* Gene Delivery. *Pharm. Res.* **2004**, *21*, 365–371.
96. Kulkarni, R. P.; Mishra, S.; Fraser, S. E.; Davis, M. E. Single Cell Kinetics of Intracellular, Nonviral, Nucleic Acid Delivery Vehicle Acidification and Trafficking. *Bioconjugate Chem.* **2005**, *16*, 986–994.
97. Ting, C. L.; Wang, Z.-G. Interactions of a Charged Nanoparticle with a Lipid Membrane: Implications for Gene Delivery. *Biophys. J.* **2011**, *100*, 1288–1297.
98. Grandinetti, G.; Smith, A. E.; Reineke, T. M. Membrane and Nuclear Permeabilization by Polymeric pDNA Vehicles: Efficient Method for Gene Delivery or Mechanism of Cytotoxicity? *Mol. Pharm.* **2011**, *9*, 523–538.
99. Zhou, J.; Liu, J.; Cheng, C. J.; Patel, T. R.; Weller, C. E.; Piepmeyer, J. M.; Jiang, Z.; Saltzman, W. M. Biodegradable Poly(amine-co-ester) Terpolymers for Targeted Gene Delivery. *Nat. Mater.* **2012**, *11*, 82–90.
100. Brewer, C. F.; Miceli, M. C.; Baum, L. G. Clusters, Bundles, Arrays and Lattices: Novel Mechanisms for Lectin-Saccharide-Mediated Cellular Interactions. *Curr. Opin. Struct. Biol.* **2002**, *12*, 616–623.
101. Seelenmeyer, C.; Wegehingel, S.; Tews, I.; Kunzler, M.; Aebi, M.; Nickel, W. Cell Surface Counter Receptors are Essential Components of the Unconventional Export Machinery of Galectin-1. *J. Cell Biol.* **2005**, *171*, 373–381.
102. Nakahara, S.; Oka, N.; Wang, Y.; Hogan, V.; Inohara, H.; Raz, A. Characterization of the Nuclear Import Pathways of Galectin-3. *Cancer Res.* **2006**, *66*, 9995–10006.
103. Grosse, S.; Tremeau-Bravard, A.; Aron, Y.; Briand, P.; Fajac, I. Intracellular Rate-Limiting Steps of Gene Transfer Using Glycosylated Polylysines in Cystic Fibrosis Airway Epithelial Cells. *Gene Ther.* **2002**, *9*, 1000–1007.
104. Roche, A. C.; Fajac, I.; Grosse, S.; Frison, N.; Rondanino, C.; Mayer, R.; Monsigny, M. Glycofection: Facilitated Gene Transfer by Cationic Glycopolymers. *Cell. Mol. Life Sci.* **2003**, *60*, 288–297.
105. Bantel-Schaal, U.; Braspenning-Wesch, I.; Kartenberg, J. Adeno-Associated Virus Type 5 Exploits Two Different Entry Pathways in Human Embryo Fibroblasts. *J. Gen. Virol.* **2009**, *90*, 317–322.
106. Doedens, J. R.; Giddings, T. H.; Kirkegaard, K. Inhibition of Endoplasmic Reticulum-to-Golgi Traffic by Poliovirus Protein 3A: Genetic and Ultrastructural Analysis. *J. Virol.* **1997**, *71*, 9054–9064.
107. Pierini, R.; Cottam, E.; Roberts, R.; Wileman, T. Modulation of Membrane Traffic between Endoplasmic Reticulum, ERGIC and Golgi to Generate Compartments for the Replication of Bacteria and Viruses. *Semin. Cell Dev. Biol.* **2009**, *20*, 828–833.
108. Duvet, S.; Cocquerel, L.; Piliez, A.; Cacan, R.; Verbert, A.; Moradpour, D.; Wychowski, C.; Dubuisson, J. Hepatitis C Virus Glycoprotein Complex Localization in the Endoplasmic Reticulum Involves a Determinant for Retention and Not Retrieval. *J. Biol. Chem.* **1998**, *273*, 32088–32095.
109. Pelkmans, L.; Kartenberg, J.; Helenius, A. Caveolar Endocytosis of Simian Virus 40 Reveals a New Two-Step Vesicular-Transport Pathway to the ER. *Nat. Cell Biol.* **2001**, *3*, 473–483.
110. Norkin, L. C.; Kuksin, D. The Caveolae-Mediated SV40 Entry Pathway Bypasses the Golgi Complex en Route to the Endoplasmic Reticulum. *Virol. J.* **2005**, *2*, 38.
111. Rasband, W. S. *Image J*; U.S. National Institutes of Health: Bethesda, MD, USA, 1997–2007.
112. Bolte, S.; Cordelieres, F. P. A Guided Tour into Subcellular Colocalization Analysis in Light Microscopy. *J. Microsc.* **2006**, *224*, 213–232.